

## Reply to reviewer 1:

Line 74

"This study shows that the percentage of swells in the measured waves was 75 to 79% at the locations with higher percentage of swells in the northern portion of AS compared to that at the southern side."

-- Unclear, please restate.

**Reply:** Corrected as below.

This study shows that the percentage of swells in the measured waves was 75% at the southern part of AS and 79% at the northern part of AS.

Line 112

-- Chart datum is ambiguous. A chart datum is likely a mean-low-lower-water or some other tidal datum. A tidal datum is not a geodetic datum. In this era of sea level-rise consciousness, it would be nice to have the geodetic water levels quantified, but you seem unwilling to invest the effort. I don't see the advantage of belabouring this point since it's the relative change in sea level that is apparently the point of this text. Why not just avoid the technicality of understanding what a geodetic datum is, which one applies, the needed transformations from a chart or tidal datum, and just say that there is a 24 cm annual cycle in mean sea level from September to January.

**Reply:** Corrected as per suggestion. Now it is as below.

There is a 0.24 m annual cycle in mean sea level from September to January.

Line 159

"An exponential curve  $y = k.f^b$  is fitted for high-frequency part of the spectrum"

-- what is  $k.f$ ? Apparently  $k$  is a coefficient?

**Reply:** Corrected as  $kf^b$ . It is mentioned that  $k$  is coefficient.

Line 236

"Since the range of maximum spectral energy density in a year is large ( $\sim 60 \text{ m}^2/\text{Hz}$ ), each wave spectrum is normalised through dividing the spectral energy density by the maximum spectral energy density of that spectrum."

-- So you are 'normalizing' each spectra independently. Why would one do this? This complicates the utility of the spectral amplitude since each spectra has it's own unique scaling and cannot be directly compared to another spectra, nor can actual water level amplitudes be recovered from the spectra without the specific scaling.

When you say that "each wave spectrum is normalised through dividing the spectral energy density by the maximum spectral energy density of that spectrum", are you literally normalizing each individual spectrum, or are you normalizing the entire spectrogram over each year? The former is unacceptable, the latter imposes that year-to-year amplitude

comparisons must be scaled.

To the point of spectral amplitudes, you note that wave spectra have physical units ( $\text{m}^2/\text{Hz}$ ), thereby one can obtain an RMS wave height at any frequency if the spectral amplitude is known. Clearly that has been obviated by your normalization and the amplitude scale in figure 5 of [0,1].

The reader is not in a position to know how the spectral normalization is applied in time and to what extent individual spectra can be compared to each other, or that a physical measurement can be extracted from the data presented in figure 5. One of the strengths of this paper is its data coverage and analysis. To remove the ability for the reader to extract a physical amplitude from the data, or to have a uniform comparison across time is difficult to understand.

These same comments/issues apply to figure 9 and the monthly mean spectral amplitudes.

If one desires to address that "the range of maximum spectral energy density in a year is large", a conventional approach is express the spectral power in decibels.

**Reply:** Now we have presented the maximum spectral energy density used for normalising each wave spectrum in Figure 2e.

In the caption of Figure 5 and 9, the below sentence is also added.

The value used for normalizing the spectral energy density is presented in Fig. 2e.

The wave spectrum is normalised and presented only to show the predominance of wind-seas or swells. Only Figs. 5 and 9 present the normalised spectral energy density. Remaining wave spectra are not normalised ones. This is now mentioned in line 326.

Line 379

"The values for  $\alpha$  and  $\gamma$  were randomly varied within a range to find out the values for which, the theoretical spectrum best fits the measured spectrum and those values were used to plot the theoretical spectrum."

-- This issue remains unanswered. You have not specified what "randomly varied" and "over a range" mean. If your work is to be reproducible, should not you reveal the methods?

**Reply:** Now the range is given as below.

The values for  $\alpha$  and  $\gamma$  were varied from 0.0001 to 0.005 and 1.1 to 3.3 respectively to find out the values for which, the theoretical spectrum best fits the measured spectrum and those values were used to plot the theoretical spectrum.

We thank the reviewer for these comments. Now we have addressed these points in the revised manuscript. The changes are shown in the attached manuscript.

# **Wave spectral shapes in the coastal waters based on measured data off Karwar, west coast of India**

Anjali Nair M, Sanil Kumar V

Ocean Engineering Division

Council of Scientific & Industrial Research-National Institute of Oceanography

Dona Paula 403 004, Goa India

\*Correspondence to email:sanil@nio.org Tel: 0091 832 2450 327

## **Abstract**

Understanding of the wave spectral shapes is of primary importance for the design of marine facilities. In this paper, the wave spectra collected from January 2011 to December 2015 in the coastal waters of the eastern Arabian Sea using the moored directional waverider buoy are examined to know the temporal variations in the wave spectral shape. Over an annual cycle, for 31.15% of the time, peak frequency is between 0.08 and 0.10 Hz and the significant wave height is also relatively high ( $\sim 1.55$  m) for waves in this class. The slope of the high-frequency tail of the monthly average wave spectra is high during the Indian summer monsoon period (June-September) compared to other months and it increases with increase in significant wave height. There is not much interannual variation in slope for swell dominated spectra during the monsoon, while in the non-monsoon period, when wind-seas have much influence, the slope varies significantly. Since the exponent of the high-frequency part of the wave spectrum is within the range from -4 to -3 during the monsoon period, Donelan spectrum shows better fit for the high-frequency part of the wave spectra in monsoon months compared to other months.

**Key Words:** Ocean surface waves, wind waves, Arabian Sea, wave spectrum, high-frequency tail

## 1. Introduction

Information on wave spectral shapes are required for designing marine structures (Chakrabarti, 2005) and almost all the wave parameters computations are based on the wave spectral function (Yuan and Huang, 2012). The growth of waves and the correspondent spectral shape is due to the complex ocean-atmosphere interactions, while the physics of air-sea interaction is not completely understood (Cavaleri et al., 2012). The shape of the wave spectrum depends on the factors governing the wave growth and decay, and a number of spectral shapes have been proposed in the past for different sea states (see Chakrabarti, 2005 for a review). The spectral shape is maintained by nonlinear transfer of energy through nonlinear four-wave interactions (quadruplet interactions) and white-capping (Gunson and Symonds, 2014). The momentum flux between the ocean and atmosphere govern the high-frequency wave components (Cavaleri et al., 2012). According to Philips, the equilibrium ranges for low-frequency and high-frequency region is proportional to  $f^5$  and  $f^4$  (where  $f$  is the frequency) respectively. Several field studies made since JONSWAP (Joint North Sea Wave Project) field campaign reveals an analytical form for wave spectra with the spectral tail proportional to  $f^4$  (Toba, 1973; Kawai et al., 1977; Kahma, 1981; Forristall, 1981; Donelan et al., 1985). Usually, there is a predominance of swell fields in large oceanic areas, which is due to remote storms (Chen et al., 2002; Hwang et al., 2011; Semedo et al., 2011). The exponent used in the expression for the frequency tail has different values (see Siadatmousavi et al., 2012 for a brief review). For shallow water, Kitaigorodskii et al. (1975) suggested  $f^{-3}$  tail, Liu (1989) suggested  $f^{-4}$  for growing young wind-seas and  $f^{-3}$  for fully developed wave spectra. Badulin et al. (2007) suggested  $f^4$  for frequencies where nonlinear interactions are dominant. The study carried out at Lake George by Young and Babanin (2006) revealed that in the frequency range  $5f_p < f < 10f_p$ , the average value of the exponent 'n' of  $f^n$  is close to 4. Whereas, some studies in real sea conditions indicate that high-frequency shape of  $f^4$  applies up to few times the peak frequency ( $f_p$ ) and then decays faster with frequency. The spectra for coastlines in Currituck Sound with short fetch condition showed a decay closer to  $f^5$  when  $f$  is greater than two or three times the peak frequency (Long and Resio, 2007). Gagnaire-Renou et al. (2010) found that the energy input from wind and dissipation due to white-capping have a significant influence on the high-frequency tail of the spectrum.

61 The physical processes in the north Indian Ocean have a distinct seasonal cycle (Shetye et  
62 al., 1985; Ranjha et al., 2015) and the surface wind-wave field is no exception (Sanil Kumar et al.,  
63 2012). In the eastern Arabian Sea (AS), significant wave height ( $H_{m0}$ ) up to 6 m is measured in the  
64 monsoon period (June to September), and during rest of the period,  $H_{m0}$  is normally less than 1.5 m  
65 (Sanil Kumar and Anand, 2004). Sanil Kumar et al. (2014) observed that in the eastern AS, the  
66 wave spectral shapes are different at two locations within 350 km distance, even though the  
67 difference in the integrated parameter like  $H_{m0}$  is marginal. Dora and Sanil Kumar (2015) observed  
68 that waves at 7-m water depth in the nearshore zone off Karwar are high energy waves in the  
69 monsoon and low to moderate waves in the non-monsoon period (January to May and October to  
70 December). Dora and Sanil Kumar (2015) study shows similar contribution of wind-seas and swells  
71 during the pre-monsoon (February to May), while swells dominate the wind-sea in the post-  
72 monsoon (October to January) and the monsoon period. A study was carried out by Glejin et al.  
73 (2012) to find the variation in wave characteristics along the eastern AS and the influence of swells  
74 in the nearshore waves at 3 locations during the monsoon period in 2010. This study shows that the  
75 percentage of swells in the measured waves was 75% at the southern part of AS and ~~to~~ 79% at the  
76 ~~locations with higher percentage of swells in the northern part~~ orion of AS ~~compared to that at the~~  
77 ~~southern side~~. Wind and wave data measured at a few locations along the west coast of India for  
78 short-period, one to two months as well as the wave model results were analysed to study the wave  
79 characteristics in the deep as well as nearshore regions during different seasons (Vethamony et al.,  
80 2013). From the wave data collected for two years period (2011 and 2012) along the eastern AS,  
81 the swells of period more than 18 s and significant wave height less than 1 m which occur for 1.4 to  
82 3.6% of the time were separated and their characteristics were studied by Glejin et al. (2016).  
83 Anjali Nair and Sanil Kumar (2016) presented the daily, monthly, seasonal and annual variations in  
84 the wave spectral characteristics for a location in the eastern AS and reported that over an annual  
85 cycle, 29 % of the wave spectra are single-peaked spectra and 71 % are multi-peaked spectra.  
86 Recently Amrutha et al. (2017) by analysing the measured wave data in October reported that the  
87 high waves (significant wave height  $> 4$  m) generated in an area bounded by 40-60° S and 20-40° E  
88 in the south Indian Ocean reached the eastern AS in 5-6 days and resulted in the long-period waves.  
89 The earlier studies indicate that the spectral tail of the high-frequency part shows large variation  
90 and its variation with seasons are not known. Similarly, the shape of the parametric spectra are also  
91 different and hence it is important to identify the spectral shapes based on the measured data  
92 covering all the seasons and different years.

The discussion above shows that there is a strong inspiration to study the high-frequency tail of the wave spectrum. For the present study, we used the directional waverider buoy measured wave spectral data at 15-m water depth off Karwar, west coast of India, over 5 years during 2011 to 2015 and evaluated the nearshore wave spectral shapes in different months. This study addresses two main questions: (1) How the high-frequency tail of the wave spectrum varies in different months, and (2) What are the spectral parameters for the best-fit theoretical spectra. This paper is organized as follows: the study area is introduced in section 2, details of data used and methodology in section 3. Section 4 presents the results of the study and the conclusions are given in section 5.

## 2. Study area

The coastline at Karwar is  $24^\circ$  inclined to the west from the north, and the 20 m depth contour is inclined  $29^\circ$  to the west. Hence, large waves in the nearshore will have an incoming direction close to  $241^\circ$ , since waves get aligned with the depth contour due to refraction. At 10, 30 and 75 km distance from Karwar, the depth contours of 20, 50 and 100 m are present (Fig. 1). The study region is under the seasonally reversing monsoon winds, with winds from the northeast during the post-monsoon and from the southwest during the monsoon period. The monsoon winds are strong and the total seasonal rainfall is 280 cm. ~~There is a 0.24 m annual cycle in mean sea level from September to January. average monthly sea level at Karwar varies from 1.06 m (in September) to 1.3 m (in January) with respect to chart datum and t~~The average tidal range is 1.58 m during spring tides and 0.72 m during neap tides (Sanil Kumar et al., 2012).

## 3. Data and methods

The waves off Karwar ( $14^\circ 49' 56''$  N and  $74^\circ 6' 4''$  E) were measured using the directional waverider buoy (DWR-MKIII) . Measurements are carried out from 1 January 2011 to 31 December 2015. The data of heave and two translational motion of the buoy are sampled at 3.84 Hz. A digital high-pass filter with a cut off at 30 s is applied to the 3.84 Hz samples. At the same time it converts the sampling rate to 1.28 Hz and stores the time series data at 1.28 Hz. From the time series data for 200s, the wave spectrum is obtained through a fast Fourier transform (FFT).

During half an hour 8 wave spectra of a 200 s data interval each are collected and averaged to get a representative wave spectrum for half an hour (Datawell, 2009). The wave spectrum is with a resolution of 0.005 Hz from 0.025 Hz to 0.1 Hz and is 0.01 Hz from 0.1 to 0.58 Hz. Bulk wave parameters; significant wave height ( $H_{m0}$ ) which equals  $4\sqrt{m_0}$  and mean wave period ( $T_{m02}$ ) based on second order moment, which equals  $\sqrt{m_0/m_2}$  are obtained from the spectral moments. Where  $m_n$  is the  $n^{\text{th}}$  order spectral moment ( $m_n = \int_0^\infty f^n S(f) df$ ,  $n=0$  and  $2$ ),  $S(f)$  is the spectral energy density and  $f$  is the frequency. The spectral peak period ( $T_p$ ) is estimated from the wave spectrum and the peak wave direction ( $D_p$ ) is estimated based on circular moments (Kuik et al., 1988). The wind-seas and swells are separated through the method described by Portilla et al. (2009) and the wind-sea and the swell parameters are computed by integrating over the respective spectral parts. Measurements reported here are in Coordinated Universal Time (UTC), which is 05:30 h behind the local time.  $U_{10}$  is the wind speed at 10-m height obtained from reanalysis data of zonal and meridional components at 6 hourly intervals from NCEP / NCAR (Kalnay et.al., 1996) and is used to study the influence of wind speed on the spectral shape.

Since the frequency bins over which the wave spectrum estimated is same in all years, the monthly and seasonally averaged wave spectrum is computed by taking the average of the spectral energy density at the respective frequencies of each spectrum over the specified time.

Wave spectrum continues to develop through non-linear wave-wave interactions even for very long times and distances. Hence, most of the wave spectrum is not fully developed and cannot be represented by Pierson-Moskowitz (PM) spectrum (Pierson and Moskowitz, 1964). Accordingly, an additional factor was added to the PM spectrum in order to improve the fit to the measured spectrum. The JONSWAP spectrum (Hasselmann et al., 1973) is thus a PM spectrum multiplied by an extra peak enhancement factor  $\gamma$ . The high-frequency tail of the JONSWAP spectrum decays in a form proportional to  $f^{-5}$ . A number of studies reported that high-frequency decay is by a form proportional to  $f^{-4}$ . Modified JONSWAP spectrum including Toba's formulation of saturation range was proposed by Donelan et al. (1985). The JONSWAP and Donelan spectrum used in the study are given in eqns. (1) and (2).

$$S(f) = \frac{\alpha g^2}{(2\pi)^4 f^5} \exp \left[ -\frac{5}{4} \left( \frac{f}{f_p} \right)^{-4} \right] \gamma^{\exp \left[ -\frac{(f-f_p)^2}{2\sigma^2 f_p^2} \right]} \quad \text{..... (1)}$$

$$S(f) = \frac{\alpha g^2}{(2\pi)^4 f^4 f_p} \exp \left[ -\left( \frac{f}{f_p} \right)^{-4} \right] \gamma^{\exp \left[ -\frac{(f-f_p)^2}{2\sigma^2 f_p^2} \right]} \quad \text{.....(2)}$$

Where  $\gamma$  is the peak enhancement parameter;  $\alpha$  is Philip's constant;  $f$  is the wave frequency;  $g$  is the gravitational acceleration and  $\sigma$  is the width parameter.

$$\sigma = \begin{cases} 0.07, & f < f_p \\ 0.09, & f \geq f_p \end{cases}$$

An exponential curve  $y = k \cdot f^b$  is fitted for high-frequency part of the spectrum and the exponent (value of  $b$ ) and the coefficient  $k$  is estimated for the best fitting curve based on statistical measures such as least square error and bias. The slope of the high-frequency part of the wave spectrum is represented by the exponent of the high-frequency tail.

For the present study, JONSWAP spectrum is tested by fitting for the whole frequency range of the measured wave spectrum. It is found out that the JONSWAP spectra do not show a good fit for higher frequency range, whereas Donelan spectrum shows better fit for the high-frequency range. Hence, JONSWAP spectrum is used for the lower frequency range up to spectral peak and Donelan spectrum is used for the higher frequency range from the spectral peak for single-peaked wave spectrum. Theoretical wave spectra are not fitted to the double-peaked wave spectra.

## 4. Results and discussions

### 4.1 Bulk wave parameters

Mostly the wave conditions ( $\sim 75\%$ ) at the buoy location are intermediate and shallow-water waves (where water depth is less than half the wavelength,  $d < L/2$ ), this condition is not satisfied during  $\sim 25\%$  of the time due to waves with mean periods of 4.4 s or less. This study,



therefore, deals with shallow, intermediate and deepwater wave climatology. Hence, bathymetry will significantly influence the wave characteristics.

The persistent monsoon winds generate choppy seas with average wave heights of 2 m and mean wave period of 6.5 s. Fig. 2 shows that in the monsoon, the observed waves had a maximum  $H_{m0}$  of about 5 m, with  $H_{m0}$  of 2-2.5 m more common during this period. The maximum  $H_{m0}$  measured during the study period is on 21 June 2015 17:30 UTC (Fig. 2a). Mean wave periods ( $T_{m02}$ ) at the measurement location ranged from 4-8 s (Fig. 2b). Wave direction during monsoon is predominantly from the west due to refraction towards the coast. The fluctuation in  $H_{m0}$  due to the southwest monsoon is seen in all the years (Fig. 2a). High waves ( $H_{m0} > 2$  m) during 27-29 November 2011 are due to the deep depression ARB04 formed in the AS. During the study period, the annual average  $H_{m0}$  is same ( $\sim 1.1$  m) in all the years (Table 1). In 2013, the data during August could not be collected and hence resulted in lower annual average  $H_{m0}$ . Over the 5 years, small waves ( $H_{m0} < 1$  m) account for a large proportion (63.94%) of measured data and only during 0.16% of the time,  $H_{m0}$  exceeded 4 m (Table 2). The 25<sup>th</sup> and 75<sup>th</sup> percentiles of the  $H_{m0}$  distribution over the entire analysis period are 0.6 and 1.4 m.

Waves with low heights ( $H_{m0} < 1$  m) are with the mean period in a large range (2.7-10.5 s), whereas high waves ( $H_{m0} > 3$  m) have mean wave period in a narrow range (6.1-9.3 s) (Table 2). For waves with  $H_{m0}$  higher than 3 m, the  $T_p$  never exceeded 14.3 s and for waves with  $H_{m0}$  less than 1 m,  $T_p$  up to 22.2 s are observed (Fig. 2c) and the long period swells (14-20 s) are with  $H_{m0} < 2.5$  m. Around 7% of the time during 2011-2015, waves have peak period more than 16.7 s (Table 3). Peak frequencies between 0.08 and 0.10 Hz, equivalent to a peak wave period of 10 - 12.5 s are observed 31.15% of the time and the  $H_{m0}$  is also relatively high ( $\sim 1.55$  m) for waves in this class. During the annual cycle, the wave climate is dominated by low ( $0.5 > H_{m0} > 1$  m) intermediate-period ( $T_p \sim 10$ -16s) south-westerly swell. Waves from the northwest are with  $T_p$  less than 8 s (Fig. 3).

The wave roses during 2011-2015 indicate that around 38% of the time during the period 2011 to 2015, the predominant wave direction is SSW (225°) with long period (14 - 18s) and intermediate period (10 - 14s) waves (Fig. 3). A small percentage of long-period waves having  $H_{m0}$  more than 1m are observed from the same direction in which more than 80% are swells (Fig. 3c).

212 Intermediate period waves observed having  $H_{m0}$  less than 1m, contain 20 - 60% of swells. Around  
213 10-15% of the waves observed during the period are from the west, which includes intermediate  
214 and short period waves with  $H_{m0}$  varying from 1.5 to 3m. These intermediate period waves from  
215 west having  $H_{m0}$  between 2.5 - 3m contain more than 80% of swells. Waves from NW are short  
216 period waves with  $H_{m0}$  between 0.5 and 1.5; in which swell percentage is very less showing the  
217 influence of wind-sea (Fig. 3d). High waves observed in the study area consists of more than 80%  
218 swells.

219  
220 Date versus year plots of significant wave height (Fig. 4) shows that  $H_{m0}$  has its maximum  
221 values ( $H_{m0} > 3m$ ) during the monsoon period with a wave direction of WSW and peak wave period  
222 of 10 - 12s (intermediate period). The mean wave period shows its maximum values (6 - 8s) during  
223 the monsoon period. During January–May in all the years,  $H_{m0}$  is low ( $H_{m0} < 1m$ ) with waves from  
224 SW, W and NW directions. NW waves observed are the result of strong sea breezes existing during  
225 this period. Both long-period ( $T_p > 14s$ ), intermediate-period ( $10 < T_p < 14s$ ) and short-period ( $T_p$   
226  $< 8s$ ) waves are observed during this period and hence, the mean wave period observed is low  
227 compared to the monsoon (Fig. 4d). During October to December, similar to the pre-monsoon  
228 period,  $H_{m0}$  observed is less than 1m, but the wave direction is predominantly from SW and W, with  
229 least NW waves. Short period waves are almost absent during this period, and the condition is  
230 similar for all the years. The interannual variations in  $H_{m0}$  are less than 15% (Fig. 4). Primary  
231 seasonal variability in waves is due to the monsoonal wind reversal. During January-March, there is  
232 a shift in the occurrences of northwest swells.

#### 233 234 4.2 Wave spectrum

235  
236 ~~Normalisation of the wave spectrum is done to know the spread of energy in different~~  
237 ~~frequencies. Since the range of maximum spectral energy density in a year is large ( $\sim 60 m^2/Hz$ ),~~  
238 ~~each wave spectrum is normalised through dividing the spectral energy density by the maximum~~  
239 ~~spectral energy density of that spectrum.~~ The normalized wave spectral energy density contours are  
240 presented for different years to know the wind-sea/swell predominance (Fig. 5). Normalisation of  
241 the wave spectrum is done to know the spread of energy in different frequencies. Since the range of  
242 maximum spectral energy density in a year is large ( $\sim 60 m^2/Hz$ ), each wave spectrum is  
243 normalised through dividing the spectral energy density by the maximum spectral energy density of  
244 that spectrum. The predominance of both the wind-seas and swells are observed in the non-

monsoon period, whereas in the monsoon only swells are predominant (Fig. 5). The separation of swells and wind-seas indicates that over an annual cycle, around 54% of the waves are swells. Glejin et al. (2012) reported that the dominance of swells during monsoon is due to the fact that even though the wind at the study region is strong during monsoon, the wind over the entire AS also will be strong and when these swells are added to the wave system at the buoy location, the energy of the swell increases (Donelan, 1987) and will result in dominance of swells. The spread of spectral energy to higher frequencies (0.15 to 0.25 Hz) is predominant during January-May (Fig. 5) due to sea-breeze in the pre-monsoon period (Neetu et al., 2006; Dora and Sanil Kumar, 2015). In the monsoon during the wave growth period, the spectral peak shifts from 0.12-0.13 Hz to 0.07-0.09 Hz (lower frequencies).

An interesting phenomenon is that the long-period ( $> 18$  s) swells are present for 2.5% of the time during the study period. The buoy location at 15 m water depth is exposed to waves from northwest to south with the nearest landmass at  $\sim 1500$  km in the northwest (Asia),  $\sim 2500$  km in the west (Africa),  $\sim 4000$  km in the southwest (Africa) and  $\sim 9000$  km in the south (Antarctica) (Amrutha et al., 2017). Due to its exposure to the Southern Oceans and the large fetch available, swells are present all year round in the study area and the swells are dominant in the non-monsoon (Glejin et al., 2013). Throughout the year, waves with period more than 10 s (low-frequency  $< 0.1$  Hz waves) are the southwest swells whereas with seasons the direction of short-period waves changes (Fig. 5). Amrutha et al. (2017) reported that the long-period waves observed in the eastern AS are the swells generated in the south Indian Ocean. In the monsoon season, the waves with high-frequency are predominantly from west-southwest, whereas in the non-monsoon they are from the northwest. In the non-monsoon period, the predominance of wind-seas and swells fluctuated and hence the mean wave direction also changed frequently (Fig. 5). The average direction of waves with  $H_{m0} < 1$  m shows the northwest wind-seas and the southwest swells, whereas, for high waves ( $H_{m0} > 3$  m), the difference between the swell and wind-sea direction decreases. This is because the high waves get aligned to the bottom contour before 15 m water depth on its approach to the shallow water.

The interannual changes of wave spectral energy density for different months in the period 2011-2015 are studied by computing the monthly average wave spectra for all the years (Fig. 6). In the non-monsoon period, the wave spectra observed is double-peaked, indicating the presence of

277 wind-seas and swells, whereas during the monsoon, due to the strong southwest winds, single  
278 peaked spectrum is observed, i.e. the swell peak with low-frequency and high spectral energy  
279 density. Along the Indian coast, Harish and Baba (1986), Rao and Baba (1996) and Sanil Kumar et  
280 al. (2003) found out that wave spectra are generally multi peaked and that the double peaked wave  
281 spectra are more frequent during low-sea states (Sanil Kumar et al., 2004). Sanil Kumar et al.  
282 (2014), Sanil Kumar and Anjali (2015) and Anjali and Sanil Kumar (2016) have also observed that  
283 double-peaked spectrum in the monsoon period in the eastern AS are due to the locally generated  
284 wind-seas and the south Indian Ocean swells. In the study area, from January to May and October  
285 to December, the swell peak is between the frequencies 0.07 and 0.08 Hz ( $12.5 < T_p < 14.3s$ ), but  
286 in the monsoon period, the swell peak is around 0.10 Hz, in all the years studied. This shows long-  
287 period swells ( $T_p > 13s$ ) in the non-monsoon period and intermediate period swells ( $8 < T_p < 13s$ )  
288 in the monsoon. Glejin et al. (2016), also observed the presence of low-amplitude long-period  
289 waves in the eastern AS in the non-monsoon period and intermediate period waves in the monsoon  
290 period. This is because of the propagation of swells from the southern hemisphere is more visible  
291 during the non-monsoon period due to the calm conditions (low wind-seas) prevailing in the eastern  
292 AS. Whereas during the monsoon period, these swells are less due to the turbulence in the north  
293 Indian Ocean (Glejin et al., 2013). Large interannual variations are observed for monthly average  
294 wave spectrum in all months except in July. This is because July is known to be the roughest month  
295 over the entire annual cycle and southwest monsoon reaches its peak during July. Hence, the  
296 influence of temporally varying wind-seas on the wave spectrum is least during July compared to  
297 other months. Due to the early onset (on 1 June) and advancement of monsoon during 2013  
298 compared to other years, the monthly average value of the maximum spectral energy is observed in  
299 June 2013 (Fig. 6). The wave spectra of November 2011 is distinct from that of other years, with  
300 low wind-sea peak frequency, i.e. 0.13 Hz due to the deep depression ARB04, occurred south of  
301 India near Cape Comorin, during 26 November–1 December, with a sustained wind speed of 55  
302 km/h. During October 2014, the second peak is observed at 0.11 Hz with comparatively high  
303 energy showing the influence of cyclonic storm NILOFAR. It is an extremely severe cyclonic  
304 storm that occurred during the period 25-31 October 2014, originated from a low-pressure area  
305 between Indian and Arabian Peninsula, with the highest wind speed of 215 km/h and affected the  
306 areas of India, Pakistan and Oman. Significant interannual variation is observed in the wind-sea  
307 peak frequency. Wave spectra averaged over each season (Fig. 7) shows that the interannual  
308 variations in energy spectra averaged over full year period almost follows the pattern of wave

spectra averaged over monsoon period, indicating the strong influence of monsoon winds over the wave energy spectra in the study area. Interannual variations within the spectrum are more for wind-sea region compared to swell region. During the study period, the maximum spectral energy observed is during 2011 monsoon.

For different frequencies, the monthly average wave direction is shown in Fig. 8. It is observed that throughout the year the mean wave direction of the swell peak is southwest (200-250°). In the non-monsoon period, the wind-sea direction is northwest (280-300°), except in October and November. This is due to the wind-seas produced by sea breeze which has the maximum intensity during the pre-monsoon season. Interannual variability in wave direction is highest during October and November, where the wind-seas from southwest direction are also observed. This is because, during these months, the wind speed and the strength of the monsoon swell decreases, which makes the low energy wind-seas produced by the withdrawing monsoon winds more visible.

Contour plots of spectral energy density (normalized) clearly show the predominance of wind-seas and swells during the non-monsoon period (Fig. 9). Only Figs. 5 and 9 present the normalised spectral energy density. In the monsoon period, the spectral energy density is mainly confined to a narrow frequency range (0.07-0.14 Hz) and the wave spectra are mainly single peaked with maximum energy within the frequency range 0.08-0.10 Hz, having direction 240°. Glejin et al. (2012) reported that in the monsoon season, the spectral peak is between 0.08 and 0.10 Hz (12-10s) for ~ 72% of the time in the eastern AS. Earlier studies also reported dominance of swells in the eastern AS during the monsoon (Sanil Kumar et al., 2012; Glejin et al., 2012). Above 0.15 Hz, energy gradually decreases, with the lowest energy observed between 0.30 and 0.50 Hz. Wind-sea energy is comparatively low during October, November and December and occurs mostly in the frequency range less than 0.20 Hz, whereas, during January-May, the frequency exceeds 0.20 Hz. In the pre-monsoon period, wind-sea plays a major role in nearshore wave environment (Rao and Baba, 1996). Wind-sea energy is found to be low during April 2015 (Fig. 6), because of reduction in local winds. The occurrence of wind-seas is very less during most of the time in November except during 2011, due to the deep depression ARB04.

340 The behavior of the high-frequency part of the spectrum is governed by the energy balance  
 341 of waves generated by the local wind fields. When the wind blows over a long fetch or for a long  
 342 time, the wave energy for a given frequency reaches the equilibrium range and the energy input  
 343 from the wind is balanced by energy loss to lower frequencies and by wave breaking (Torsethaugen  
 344 and Haver, 2004). The high-frequency tail slope of the monthly average wave spectrum in different  
 345 years shows that the slope is high ( $b < -3.1$ ), during June to September and the case is same for all  
 346 the years studied (Table 4). During all other months, the exponent in the expression for the  
 347 frequency tail is within the range - 3.1 to -1.5. The distribution of exponent values for different  
 348 significant wave height ranges shows that the slope increases (exponent decrease from -2.44 to -  
 349 4.20) as the significant wave height increases and reaches a saturation range. For frequencies from  
 350 0.23 to 0.58 Hz in the eastern AS during January-May, Amrutha et al. (2017) observed that the  
 351 high-frequency tail has  $f^{2.5}$  pattern at 15 m water depth and for frequencies ranging from 0.31 to  
 352 0.55 Hz, the high-frequency tail follows  $f^3$  at 5 m water depth. Since  $H_{m0}$  is maximum during the  
 353 monsoon period, the slope is also maximum during June to September. There is no much  
 354 interannual variation in slope for swell dominated spectra during the monsoon, while in the non-  
 355 monsoon period when wind-seas have much influence, the slope varies significantly.

356  
 357 The most obvious manifestations of nonlinearity are sharpening of the wave crests and the  
 358 flattening of the wave troughs and these effects are reflected in the skewness of the sea surface  
 359 elevation (Toffoli, 2006). Zero skewness indicates linear sea states, positive skewness value  
 360 indicate that the wave crests are bigger than the troughs. Figure 10 shows that nonlinearity  
 361 increases with increase in  $H_{m0}$ . The slope of the high-frequency end of the wave spectrum becomes  
 362 steeper when the wave nonlinearity increases. Donelan et al. (2012) find that in addition to the  $k^{-4}$   
 363 dissipation that swells modulate the equilibrium in breaking waves dependent on the mean surface  
 364 slope, while Melville (1994) also quantified a relation between wave packet slopes and dissipation  
 365 rate. These results are specific to breaking waves, but one might expect similar relations between  
 366 surface dynamics and dissipation rate for non breaking waves. A function of the form:  $A * \exp(\lambda$   
 367  $H_{m0}) + s_0$ , with initial parameters of  $A = 8$ ,  $\lambda = -2.4$ ,  $s_0 = -3.7$  is found to fit the exponent of the  
 368 high-frequency tail data with the significant wave height (Fig. 11a). The functional representation  
 369 of the exponent of the high-frequency tail data with  $H_{m0}$  shown in Fig. 11a might be useful in  
 370 revealing the physical connection, and at the very least would provide a predictive basis relating  
 371 spectral slopes with mean significant wave heights as a basis for future research. It is shown in Fig.

11b that the exponent decreases (slope increases) as the mean wave period increases. The study shows that the tail of the spectrum is influenced by the local wind conditions (Fig. 11c) and the influence is more with the zonal component (u) of the wind than on the meridional component (v) (Figs. 11e and 11f). The exponent of the high-frequency tail decreases with the increase of the inverse wave age ( $U_{10}/c$ ), where c is the celerity of the wave.

#### 4.3 Comparison with theoretical wave spectra

In the monsoon period, the spectrum is single peaked with high spectral energy density and during this period JONSWAP spectrum is fitted up to the peak frequency and after that Donelan spectrum is used. The monthly average wave spectra during the monsoon period for the year 2011, is compared with JONSWAP and Donelan theoretical wave spectra in Figure 12. It is found that JONSWAP and Donelan spectra with modified parameters describe well the wave spectra at low frequencies and high frequencies respectively. The values for  $\alpha$  and  $\Upsilon$  were ~~randomly-varied~~ from 0.0001 to 0.005 and 1.1 to 3.3 respectively ~~within a range~~ to find out the values for which, the theoretical spectrum best fits the measured spectrum and those values were used to plot the theoretical spectrum. The values of  $\alpha$  and  $\Upsilon$  thus obtained, for June, July, August and September are given in Table 6. From the table, the average values of  $\alpha$  and  $\Upsilon$ , for the monsoon months are obtained as 0.0009 and 1.82 for JONSWAP spectra and 0.0274 and 1.64 for Donelan spectra respectively. These values are less than the generally recommended values of  $\alpha$  and  $\Upsilon$ ; 0.0081 and 3.3.  $\alpha$  is a constant that is related to the wind speed and fetch length. For all the data, Donelan spectrum fitted is proportional to  $f^n$ , where n is the exponent value of the high-frequency tail. The theoretical spectrum JONSWAP and Donelan cannot completely describe the high-frequency tail of the measured spectrum since the high-frequency tail in these spectrum decays in the form of  $f^{-5}$  and  $f^{-4}$  respectively. Since the exponent of the high-frequency tail of the wave spectrum is within the range -4 to -3 during the monsoon period, Donelan spectrum shows better fit for monsoon spectra compared to other months (Fig. 11).

#### 5. Concluding remarks

In this paper, the variations in the wave spectral shapes in different months for a nearshore location are investigated, based on in situ wave data obtained from a moored directional waverider

404 buoy. Interannual variations within the spectrum are more for wind-seas compared to swells. The  
405 maximum significant wave height measured at 15 m water depth is 5 m and the annual average  $H_{m0}$   
406 has similar value ( $\sim 1.1$  m) in all the years. Over the 5 years, small waves ( $H_{m0} < 1$  m) account for a  
407 large proportion of measured data (63.94% of the time). The study shows that high waves ( $H_{m0} > 2$   
408 m) are with spectral peak period between 8 and 14 s and the long period swells (14-20 s) are with  
409  $H_{m0} < 2.5$  m. The high-frequency slope of the wave spectrum (the exponent decreases from -2.44 to  
410 -4.20) increases with increase in significant wave height and mean wave period. During the  
411 monsoon period, Donelan spectrum shows better fit for monsoon spectra compared to other months  
412 since the exponent of the high-frequency part of the wave spectrum is within the range -4 to -3. The  
413 decay of the high-frequency waves are fastest with depth and hence, the high-frequency tail values  
414 observed in the study will be different for different water depths.

415

## 416 **Acknowledgments**

417 The authors acknowledge the Earth System Science Organization, Ministry of Earth  
418 Sciences, New Delhi for providing the financial support to conduct part of this research. We thank  
419 TM Balakrishnan Nair, Head OSISG and Arun Nherakkol, Scientist, INCOIS, Hyderabad and Jai  
420 Singh, Technical Assistant, CSIR-NIO for the help during the collection of data. We thank Dr. Bhat  
421 and Dr. J L Rathod, Department of Marine Biology, Karnataka University PG Centre, Karwar for  
422 providing the logistics required for wave data collection. This work contributes part of the Ph.D.  
423 work of the first author. This paper is dedicated to the memory of our esteemed colleague Ashok  
424 Kumar, in recognition of his substantial contributions in initiating the long-term wave  
425 measurements in the shallow waters around India. We thank the topic editor and both the reviewers  
426 for their critical comments and the suggestions which improved the scientific content of the  
427 publication. This publication is a NIO contribution.

428

## 429 **References**

430

- 431 Amrutha, M.M., Sanil Kumar, V., and George, J.: Observations of long-period waves in the  
432 nearshore waters of central west coast of India during the fall inter-monsoon period, *Ocean*  
433 *Engineering*, 131, 244-262, 10.1016/j.oceaneng.2017.01.014, 2017.
- 434 Anjali, N.M., and Sanil Kumar, V.: Spectral wave climatology off Ratnagiri - northeast Arabian  
435 Sea, *Natural Hazards*, 82, 1565-1588, 2016.



436 Badulin, S.I., Babanin, A.V., Zakharov, V.E. and Resio, D.: Weakly turbulent laws of wind-wave  
437 growth, *Journal of Fluid Mechanics.*, 591, 339-378, 2007.

438 Cavaleri, L., Fox-Kemper, B., and Hemer, M.: Wind-waves in the coupled climate sys- tem. *Bull.*  
439 *Am. Meteorol. Soc.*, 93, 1651–1661, 2012.

440 Chakrabarti, S.K.: *Handbook of Offshore Engineering, Vol-1, Ocean Engineering Series*, Elsevier,  
441 p 661, 2005.

442 Chen, G., Chapron, B., Ezraty, R., and Vandemark, D.: A global view of swell and wind-sea  
443 climate in the ocean by satellite altimeter and scatterometer. *J. Atmospheric and Oceanic*  
444 *Technology.*, 19(11), 1849-1859, 2002.

445 Datawell.: *Datawell Waverider Reference Manual*. Datawell BV oceanographic instruments, The  
446 Netherlands, Oct. 10, pp.123, 2009.

447 Donelan, M. A.: The effect of swell on the growth of wind waves, *Johns Hopkins APL Technical*  
448 *Digest.*, 8 (1), 18-23, 1987.

449 Donelan, M., Hamilton, H., and Hui, W.H.: Directional spectra of wind-generated waves,  
450 *Philosophical Transactions of the Royal Society of London A: Mathematical, Physical and*  
451 *Engineering Sciences.*, 315(1534), 509-562, 1985.

452 Donelan, M.A., Curcic, M., Chen, S.S. and Magnusson, A.K.: Modeling waves and wind stress,  
453 *Journal of Geophysical Research: Oceans.*, 117(C11), 2012.

454 Dora, G.U., and Sanil Kumar, V.: Sea state observation in island-sheltered nearshore zone based on  
455 in situ intermediate-water wave measurements and NCEP/CFSR wind data, *Ocean Dynamics.*, 65,  
456 647-663, 2015.

457 Forristall, G.Z.: Measurements of a saturated range in ocean wave spectra, *Journal of Geophysical*  
458 *Research: Oceans.*, 86(C9), 8075-8084, 1981. Gagnaire-Renou, E., Benoit, M. and Forget, P.: Ocean  
459 wave spectrum properties as derived from quasi-exact computations of nonlinear wave-wave  
460 interactions, *Journal of Geophysical Research: Oceans.*, 115(C12), 2010.

461 Glejin, J., Sanil Kumar, V., Balakrishnan Nair, T. M., and Singh, J.: Influence of winds on  
 462 temporally varying short and long period gravity waves in the near shore regions of the eastern  
 463 Arabian Sea, *Ocean Sci.*, 9, 343–353, doi:10.5194/os-9-343-2013, 2013.

464 Glejin, J., Sanil Kumar, V., Sajiv, P.C., Singh, J., Pednekar, P., Ashok Kumar, K., Dora, G.U., and  
 465 Gowthaman, R.: Variations in swells along eastern Arabian Sea during the summer monsoon, *Open*  
 466 *J. Mar. Sci.*, 2 (2), 43–50, 2012.

467 Glejin, J., Sanil Kumar, V., Amrutha, M.M. and Singh J.: Characteristics of long-period swells  
 468 measured in the in the near shore regions of eastern Arabian Sea, *Int. J. Naval Architecture and*  
 469 *Ocean Engineering*, 8, 312-319, 2016.

470 Gunson, J., and Symonds, G.: Spectral Evolution of Nearshore Wave Energy during a Sea-Breeze  
 471 Cycle, *J. Phys. Oceanogr.*, 44(12), 3195-3208, 2014.

472 Harish, C. M., and Baba, M.: On spectral and statistical characteristics of shallow water waves,  
 473 *Ocean Eng.*, 13(3), 239-248, 1986.

474 Hasselmann, K., Barnett, T.P., Bouws, F., Carlson, H., Cartwright, D.E., Enke, K., Ewing J.A.,  
 475 Gienapp, H., Hasselmann, D.E., Krusemann, P., Meerburg, A., Muller, P., Olbers, D.J., Richter, K.,  
 476 Sell, W., and Walden, H.: Measurements of wind-wave growth and swell decay during the Joint  
 477 North Sea Wave Project (JONSWAP), *Deutsches Hydrographisches Institut.*, A8 (12), 95, 1973.

478 Hwang, P.A., Garcia-Nava, H., and Ocampo-Torres, F.J.: Dimensionally Consistent Similarity  
 479 Relation of Ocean Surface Friction Coefficient in Mixed Seas, *J. Phys. Oceanogr* 41., 1227–1238.  
 480 2011.

481 Kahma, K.K.: A study of the growth of the wave spectrum with fetch, *Journal of Physical*  
 482 *Oceanography.*, 11(11), 1503-1515, 1981.

483 Kalnay, E., Kanamitsu, M., Kistler, R., Collins, W., Deaven, D., Gandin, L., Iredell, M., Saha, S.,  
 484 White, G., Woollen, J. and Zhu, Y.: The NCEP/NCAR 40-year reanalysis project, *Bulletin of the*  
 485 *American meteorological Society.*, 77(3), 437-471, 1996.

486 Kawai, S., Okada, K. and Toba, Y.: Field data support of three-seconds power law and  $\sigma_g^4$  - 4-  
 487 spectral form for growing wind waves, *Journal of Oceanography.*, 33(3), 137-150, 1977.

488 Kitaigorodskii, S.A., Krasitskii, V.P. and Zaslavskii, M.M.: On Phillips' theory of equilibrium range  
 489 in the spectra of wind-generated gravity waves, *Journal of Physical Oceanography.*, 5(3), 410-420,  
 490 1975.

491 Kuik, A. J., Vledder, G., and Holthuijsen, L.H.: A method for the routine analysis of pitch and roll  
 492 buoy wave data, *J. Phys. Oceanogr.*, 18, 1020–1034, 1988.

493 Liu, A.K., Jackson, F.C., Walsh, E.J. and Peng, C.Y.: A case study of wave-current interaction near  
 494 an oceanic front, *Journal of Geophysical Research: Oceans.*, 94(C11), 16189-16200, 1989.

495 Long, C.E. and Resio, D.T.: Wind wave spectral observations in currituck sound, north Carolina,  
 496 *Journal of Geophysical Research: Oceans.*, 112(C5), 2007.

497 Longuet-Higgins, M.S.: On the joint distribution of the periods and amplitudes of sea waves, *J.*  
 498 *Geophys. Res.-Oceans.*, 80, 2688–2694, 1975.

499 Neetu, S., Shetye Satish., and Chandramohan, P.: Impact of sea breeze on wind-seas off Goa, west  
 500 coast of India, *Journal Earth System Science.*, 115, 229-234, 2006.

501 Pierson, W.J., and Moskowitz, L.: A proposed form for fully developed seas based on the similarity  
 502 theory of S.A.Kitaigorodski, *J. Geophys. Res.-Oceans.*, 69(24), 5181-5190, 1964.

503 Portilla, J., Ocampo-Torres, F.J., and Monbaliu, J.: Spectral Partitioning and Identification of  
 504 Wind-sea and Swell, *J. Atmospheric and Oceanic Technology.*, 26, 117-122, 2009.

505 Ranjha, R., Tjernström, M., Semedo, A., Svensson, G.: Structure and variability of the Oman  
 506 Coastal Low-Level Jet, *Tellus A*, 67, 25285, <http://dx.doi.org/10.3402/tellusa.v67.2528>, 2015.

507 Rao, C. P., and Baba, M.: Observed wave characteristics during growth and decay: a case study,  
 508 *Continental Shelf Res.*, 16(12), 1509-1520, 1996.

509 Sanilkumar, V., Ashokkumar, K. and Raju, N.S.N.: Wave characteristics off Visakhapatnam coast  
 510 during a cyclone, *Indian Academy of Sciences.*, 2004.

511 Sanil Kumar, V., Johnson, G., Dora, G.U., Chempalayil, S.P., Singh, J., and Pednekar, P.:  
 512 Variations in nearshore waves along Karnataka, west coast of India, *J. Earth Systems Science.*, 121,  
 513 393-403, 2012.

514 Sanil Kumar, V., Anand, N.M., Kumar, K.A., and Mandal, S.: Multipeakedness and groupiness of  
515 shallow water waves along Indian coast, *J. Coastal Res.*, 19, 1052-1065, 2003.

516 Sanil Kumar, V., and Anand, N.M.: Variation in wave direction estimated using first and second  
517 order Fourier coefficients, *Ocean Eng.*, 31, 2105–2119, 2004.

518 Sanil Kumar, V. and Anjali Nair, M.: Inter-annual variations in wave spectral characteristics at a  
519 location off the central west coast of India, *Ann. Geophys.*, 33, 159–167, doi:10.5194/angeo-33-  
520 159-2015, 2015.

521 Sanil Kumar, V., Shanas, P.R., and Dubhashi, K.K.: Shallow water wave spectral characteristics  
522 along the eastern Arabian Sea, *Natural Hazards*, 70, 377–394, 2014.

523 Semedo, A., Sušelj, K., Rutgersson, A., and Sterl, A.: A global view on the wind-sea and swell  
524 climate and variability from ERA-40, *J. Climate*, 24(5), 1461-1479, 2011.

525 Shetye, S.R., Shenoi, S.S.C., Antony, A.K., and Kumar, V.K.: Monthly-mean wind stress along the  
526 coast of the north Indian Ocean, *J. Earth Syst. Sci.*, 94, 129–137, doi:10.1007/BF02871945, 1985.

527 Shore Protection Manual., U.S. Army Coastal Engineering Research Center, Department of the  
528 Army, Corps of Engineers, U.S. Govt. Printing Office, Washington, DC, USA, vols. 1 and 2, 1984.

529 Siadatmousavi, S.M., Jose, F. and Stone, G.W.: On the importance of high frequency tail in third  
530 generation wave models, *Coastal Engineering.*, 60, 248-260, 2012.

531 Toba, Y.: Local balance in the air-sea boundary processes, *Journal of Oceanography.*, 29(5), 209-  
532 220, 1973.

533 Toffoli, A., Onorato, M. and Monbaliu, J.: Wave statistics in unimodal and bimodal seas from a  
534 second-order model, *European Journal of Mechanics B/Fluids*, 25, 649–661, 2006.

535 Torsethaugen, K., and Haver, S.: Simplified double peak spectral model for ocean waves, In:  
536 *Proceeding of the 14th International Offshore and Polar Engineering Conference*, 2004.

537 Vethamony, P., Rashmi, R., Samiksha, S.V. and Aboobacker, M.: Recent Studies on Wind Seas  
538 and Swells in the Indian Ocean: A Review, *International J. Ocean and Climate Systems*, 4, 63 - 73,  
539 2013.

540 Young, I.R. and Babanin, A.V.: Spectral distribution of energy dissipation of wind-generated  
541 waves due to dominant wave breaking, Journal of Physical Oceanography., 36(3), 376-394, 2006.

542 Yuan, Y., and Huang, N.E.: A reappraisal of ocean wave studies, J. Geophys. Res.-Oceans.,  
543 117(C11), 2012.

#### 544 **Figure captions**

545 Figure 1. Study area along with the wave measurement location in eastern Arabian Sea

546 ~~Figure 2. Time series plot of a) significant wave height, b) mean wave period, c) peak wave period~~  
547 ~~and d) mean wave direction from 1 January 2011 to 31 December 2015. Thick blue line indicates~~  
548 ~~the monthly average values~~

549 Figure 2. Time series plot of a) significant wave height, b) mean wave period, c) peak wave period  
550 and d) mean wave direction e) maximum spectral energy density from 1 January 2011 to 31  
551 December 2015. Thick blue line indicates the monthly average values  
552

553 Figure 3. Wave roses during 2011-2015 (a) significant wave height and mean wave direction, (b)  
554 peak wave period and mean wave direction, (c) percentage of swell, (d) percentage of wind-sea and  
555 mean wave direction

556 Figure 4. Date verses year plot of a) significant wave height b) mean wave direction, c) peak wave  
557 period and d) mean wave period

558 Figure 5. Temporal variation of normalized spectral energy density (top panel) and mean wave  
559 direction (bottom panel) with frequency in different years. The value used for normalizing the  
560 spectral energy density is presented in Fig. 2e.

561 Figure 6. Monthly average wave spectra in 2011 to 2015

562 Figure 7. Wave spectra averaged over a) pre-monsoon (February-May), b) monsoon (June-  
563 September), c) post-monsoon (October-January) and d) full year in different years

564 Figure 8. Monthly average wave direction at different frequencies in different months

565 Figure 9. Temporal variation of normalized spectral energy density in different months (data from  
566 2011 to 2015 used). The value used for normalizing the spectral energy density is presented in Fig.  
567 2e.

568 Figure 10. Scatter plot of significant wave height with skewness of the sea surface elevation in  
569 different years

570 Figure 11. Plot of exponent of the high-frequency tail with a) significant wave height, b) mean  
571 wave period, c) wind speed, d) inverse wave age, e) u-wind and f) v-wind

572 Figure 12. Fitted theoretical spectra along with the monthly average wave spectra for different  
573 month

574

575 Table 1. Number of data used in the study in different years along with range of significant wave  
576 height and average value  
577

Year	Significant wave height (m)		Number of data	%of data
	Range	Average		
2011	0.3-4.4	1.1	17517	99.98
2012	0.3-3.7	1.1	17323	98.61
2013	0.3-3.6	0.9*	14531	82.94
2014	0.3-4.5	1.1	17284	98.65
2015	0.3-5.0	1.1	14772	84.32

\* average value is estimated excluding the July month data

578  
579  
580  
581  
582  
583  
584  
585  
586

Table 2. Characteristics of waves in different range of significant wave height

Significant wave height range	Number (percentage)	Range of Tp (s)	Mean Tp (s)	Range of T <sub>m02</sub> (s)	Mean T <sub>m02</sub> (s)
$H_{m0} < 1$ m	52062 (63.94)	2.6-22.2	12.2	2.7-10.5	4.9
$1 \leq H_{m0} < 2$ m	18297 (22.47)	3.6-22.2	10.5	3.4-10.7	5.7
$2 \leq H_{m0} < 3$ m	9839 (12.08)	6.2-18.0	10.8	5.0-8.9	6.5
$3 \leq H_{m0} < 4$ m	1096 (1.35)	10.0-14.3	11.8	6.1-9.1	7.2
$4 \text{ m} \leq H_{m0}$	133 (0.16)	10.5-14.3	12.6	7.2-9.3	7.8

587  
588  
589  
590  
591  
592  
593  
594

Table 3. Average wave parameters and number of data in different spectral peak frequencies

Frequency ( $f_p$ ) range (Hz)	Number of data and %	$H_{m0}$ (m)	T <sub>m02</sub> (s)	Peak wave period (s)
$0.04 < f_p \leq 0.05$	318 (0.39)	0.73	5.24	20.19
$0.05 < f_p \leq 0.06$	5341 (6.56)	0.82	5.48	17.16
$0.06 < f_p \leq 0.07$	14764 (18.13)	0.75	5.22	14.73
$0.07 < f_p \leq 0.08$	18221 (22.38)	0.80	5.05	12.96
$0.08 < f_p \leq 0.10$	25364 (31.15)	1.55	5.76	10.88
$0.10 < f_p \leq 0.15$	9459 (11.62)	1.25	5.35	8.07
$0.15 < f_p \leq 0.20$	6355 (7.80)	0.76	4.43	5.72
$0.20 < f_p \leq 0.30$	1487 (1.83)	0.78	3.86	4.36
$0.30 < f_p \leq 0.50$	118 (0.14)	0.66	3.22	3.09

595

596  
597  
598  
599

Table 4. Exponent of the high-frequency tail of the monthly average wave spectra in different years

Months	Exponent of the high-frequency tail					
	2011	2012	2013	2014	2015	2011-2015
January	-2.08	-2.93	-2.97	-2.72	-2.81	-2.72
February	-2.41	-3.02	-2.74	-2.99	-3.06	-2.85
March	-2.75	-2.91	-2.82	-2.76	No data	-2.81
April	-2.56	-2.74	-2.64	-2.71	-2.19	-2.60
May	-2.59	-2.67	-2.63	-2.42	-2.51	-2.56
June	-3.64	-3.53	-3.55	-3.82	-3.58	-3.55
July	-3.76	-3.55	No data	-3.82	-3.63	-3.70
August	-3.63	-3.58	-3.40	-3.52	-3.65	-3.58
September	-3.41	-3.44	-3.16	-3.38	-3.00	-3.30
October	-2.02	-2.77	-3.03	-2.52	-2.61	-2.68
November	-1.78	-2.43	-1.77	-1.55	-1.65	-1.84
December	-1.69	-2.23	-1.95	-2.06	-1.79	-1.94

600  
601  
602  
603  
604  
605  
606  
607  
608  
609

Table 5. Exponent of the high-frequency tail of the average wave spectra in different wave height ranges

Range of $H_{m0}$ (m)	Exponent of the high-frequency tail
0-1	-2.44
1-2	-3.26
2-3	-3.67
3-4	-4.21
4-5	-4.21

610  
611



612 Table 6. Parameters of the fitted wave spectrum in different years  
613  
614

Year		JONSWAP spectrum		Donelan spectrum	
		$\alpha$	$\gamma$	$\alpha$	$\gamma$
2011	June	0.0013	2.2	0.0028	2.0
	July	0.0016	1.5	0.0021	1.7
	August	0.0013	1.8	0.0029	1.7
	September	0.0004	2.3	0.0021	1.6
2012	June	0.0015	1.6	0.0029	2.0
	July	0.0010	2.1	0.0031	1.9
	August	0.0009	2.2	0.0032	1.7
	September	0.0006	2.0	0.0024	1.8
2013	June	0.0006	3.3	0.0030	1.9
	July	No data			
	August	0.0012	1.1	0.0038	1.4
	September	0.0005	1.9	0.0042	1.4
2014	June	0.0010	1.1	0.0010	1.6
	July	0.0006	2.5	0.0019	1.2
	August	0.0006	1.5	0.0021	1.2
	September	0.0011	1.1	0.0032	1.4
2015	June	0.0011	1.4	0.0023	1.8
	July	0.0011	1.9	0.0024	1.8
	August	0.0008	1.8	0.0024	1.4
	September	0.0006	1.3	0.0043	1.6

615  
616

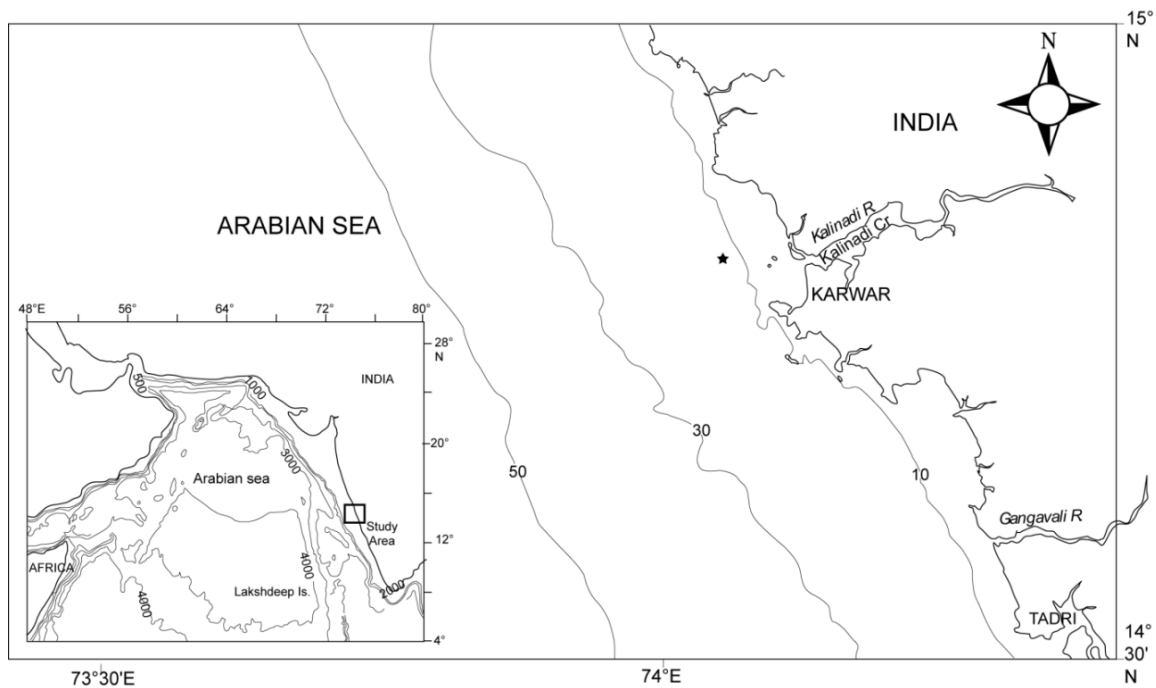
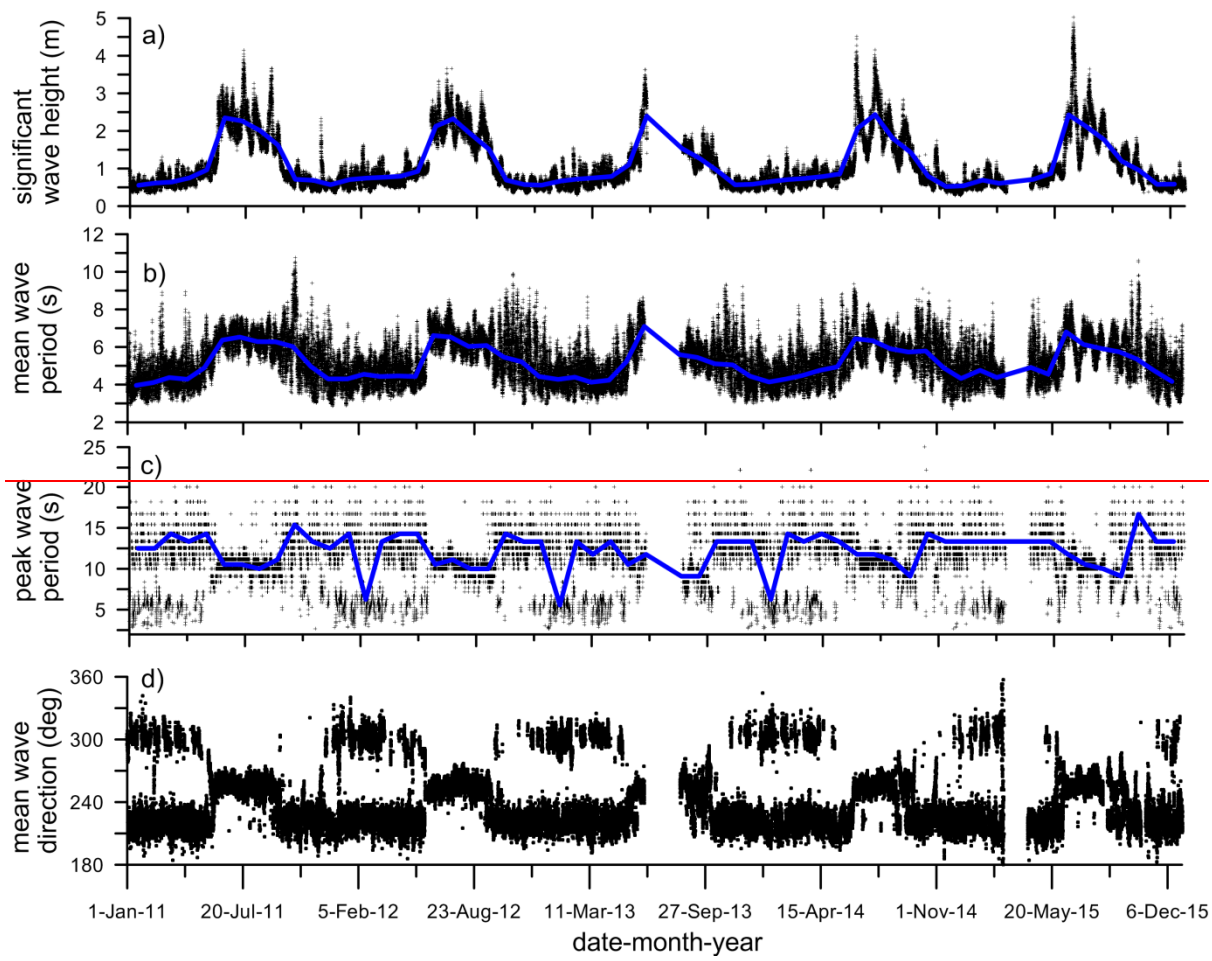


Figure 1. Study area along with the wave measurement location in eastern Arabian Sea

620  
621



622

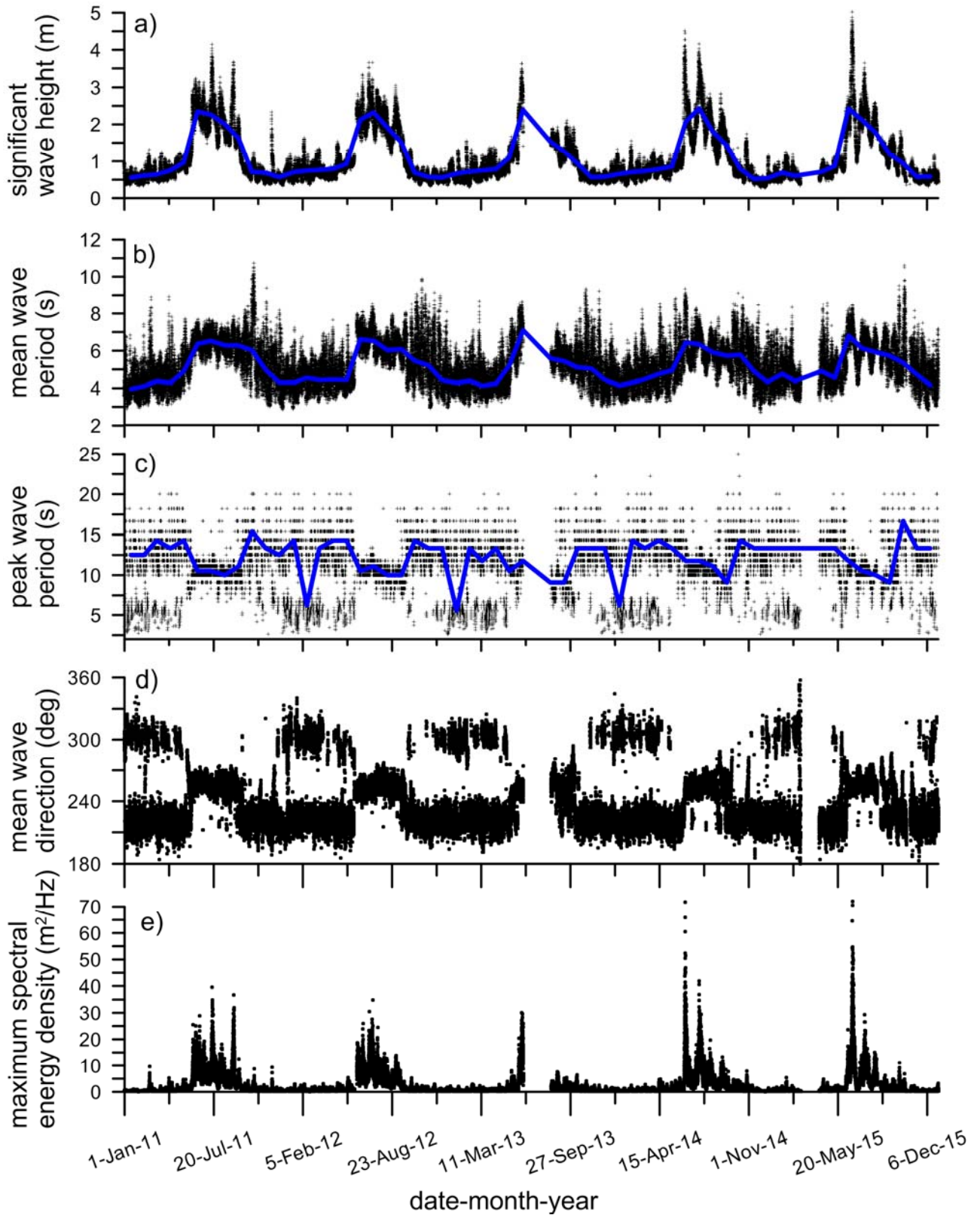


Figure 2. Time series plot of a) significant wave height, b) mean wave period, c) peak wave period and d) mean wave direction e) maximum spectral energy density from 1 January 2011 to 31 December 2015. Thick blue line indicates the monthly average values

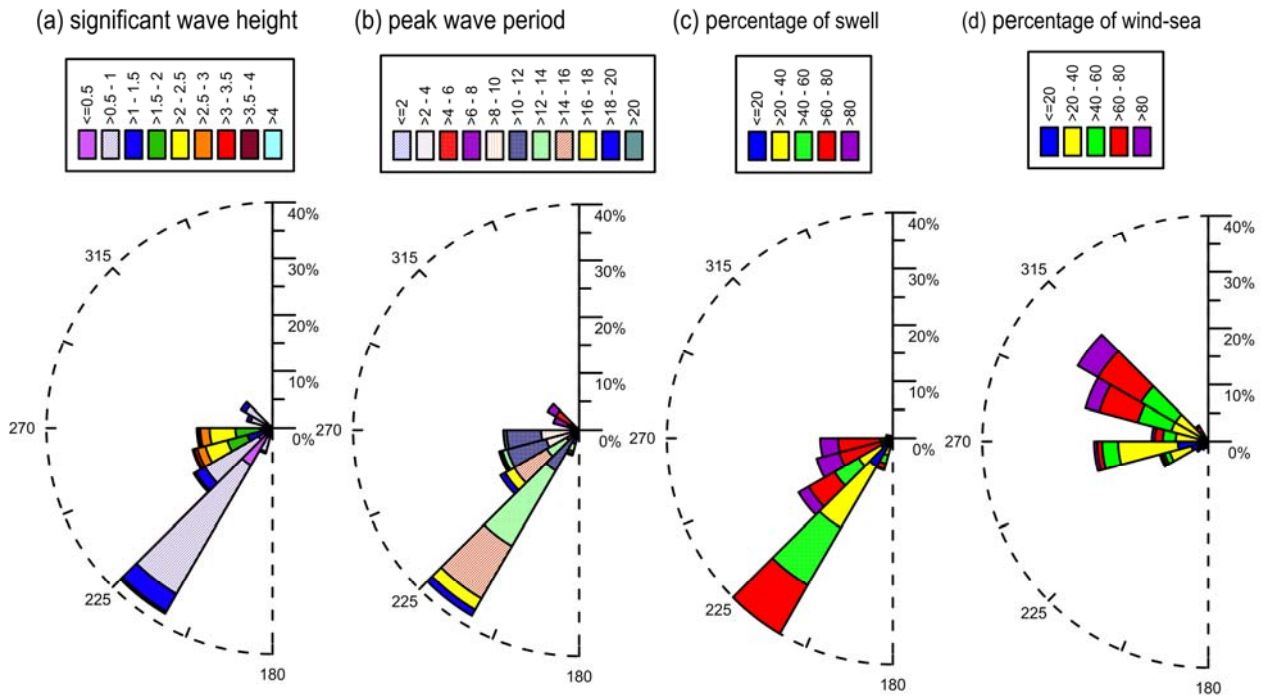
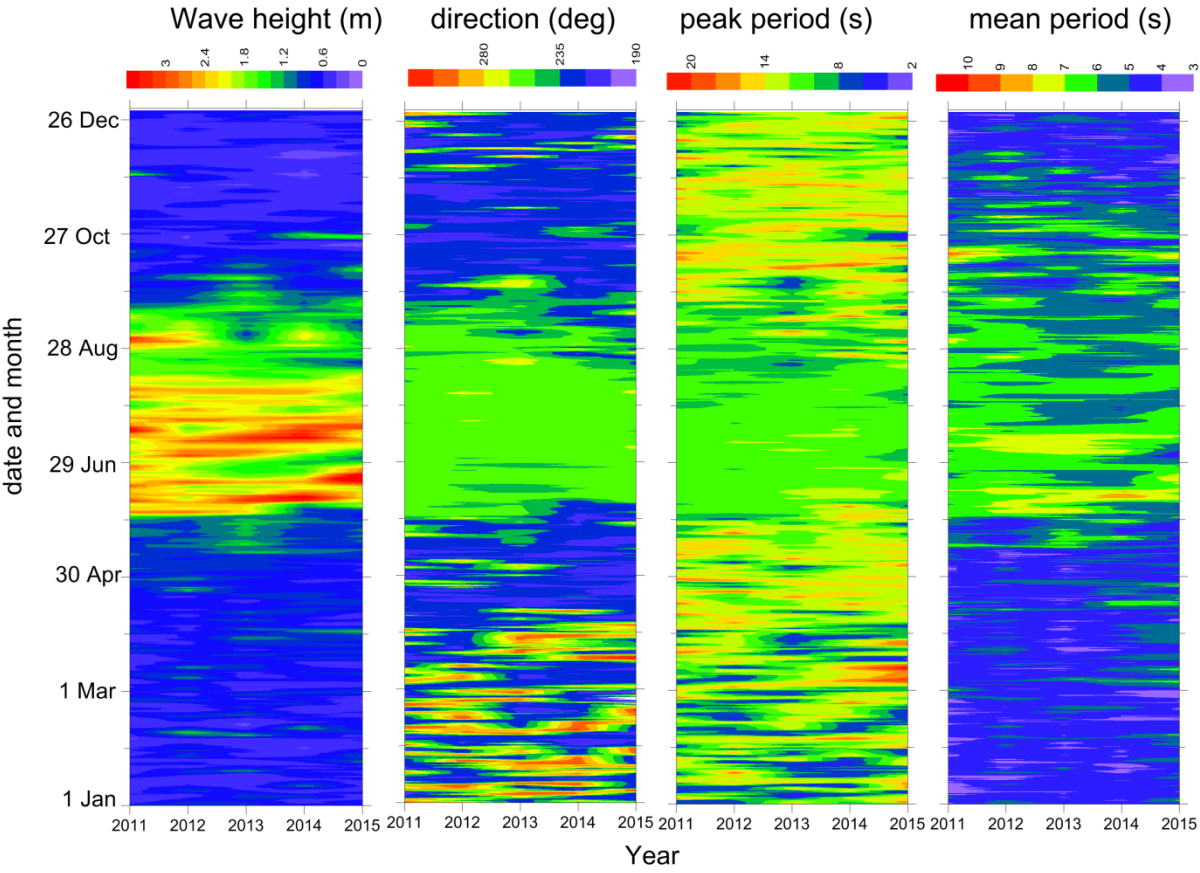


Figure 3. Wave roses during 2011-2015 (a) significant wave height and mean wave direction, (b) peak wave period and mean wave direction, (c) percentage of swell, (d) percentage of wind-sea and mean wave direction

633  
634

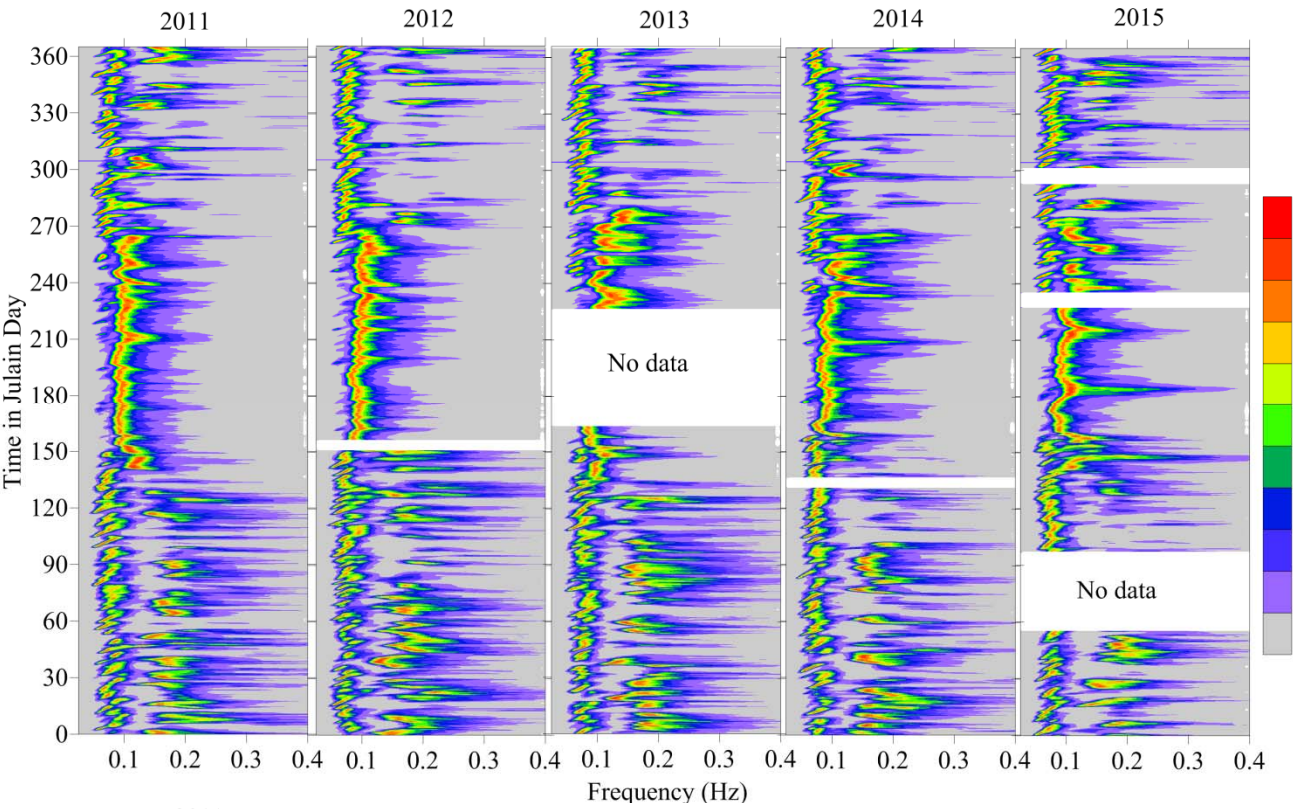


635  
636  
637  
638

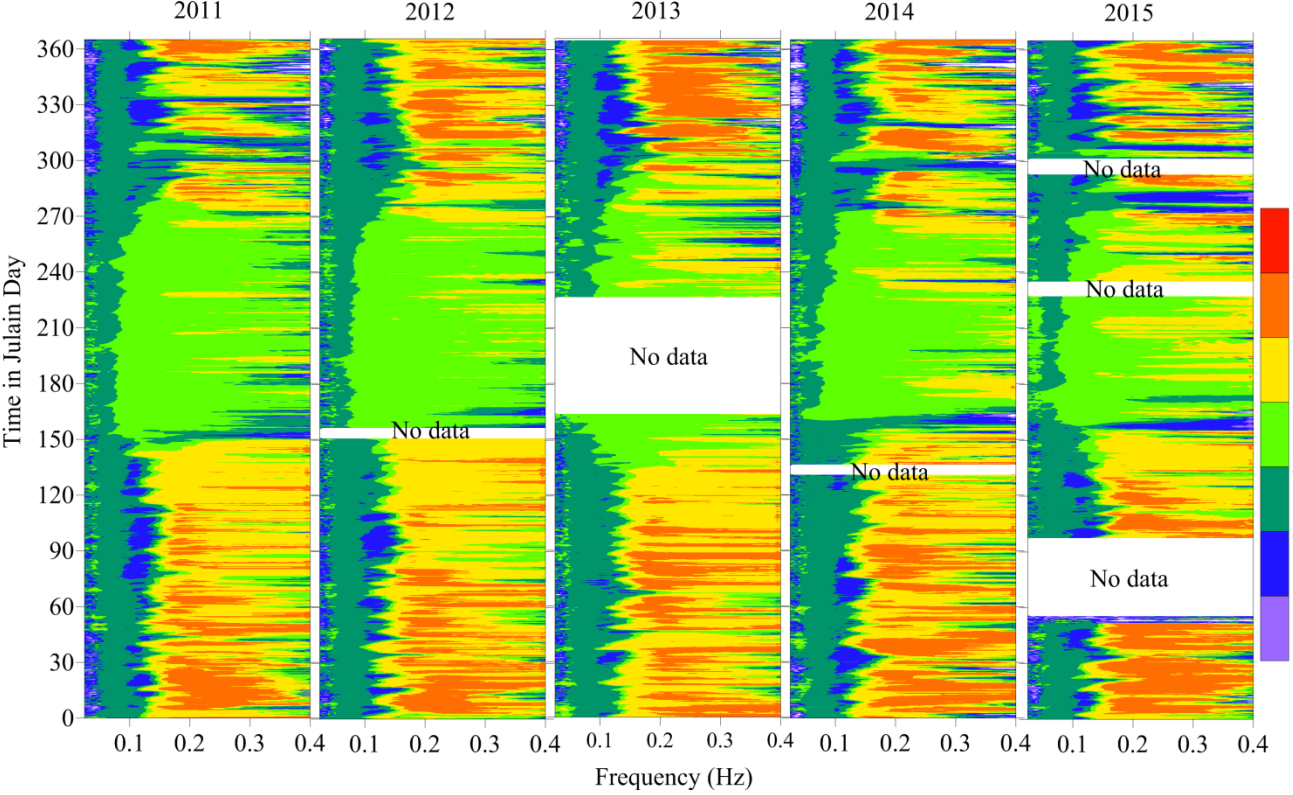
Figure 4. Date verses year plots of a) significant wave height b) mean wave direction, c) peak wave period and d) mean wave period.



639  
640



641



642  
643  
644  
645

Figure 5. Temporal variation of normalized spectral energy density (top panel) and mean wave direction (bottom panel) with frequency in different years. The value used for normalizing the spectral energy density is presented in Fig. 2e.

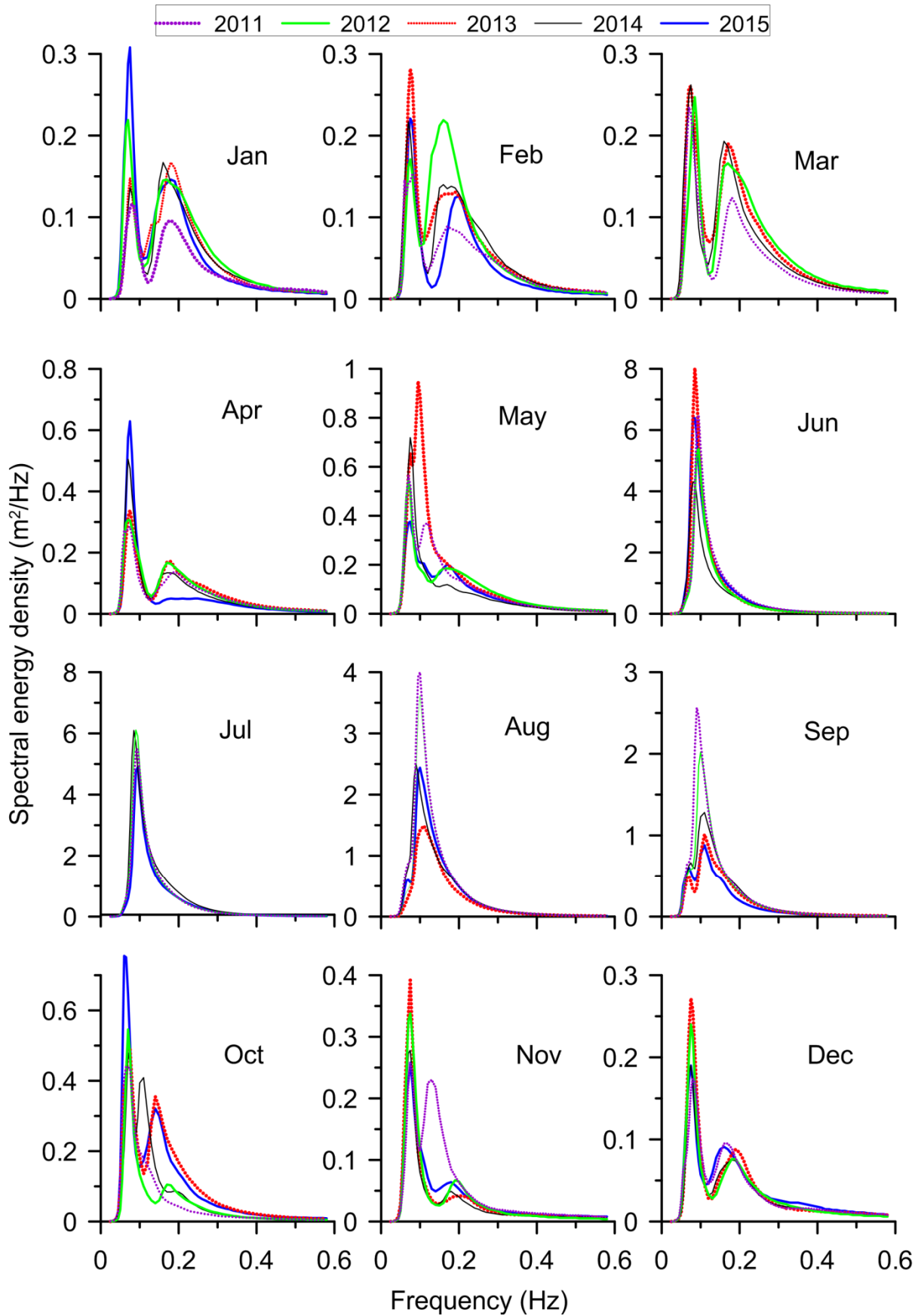
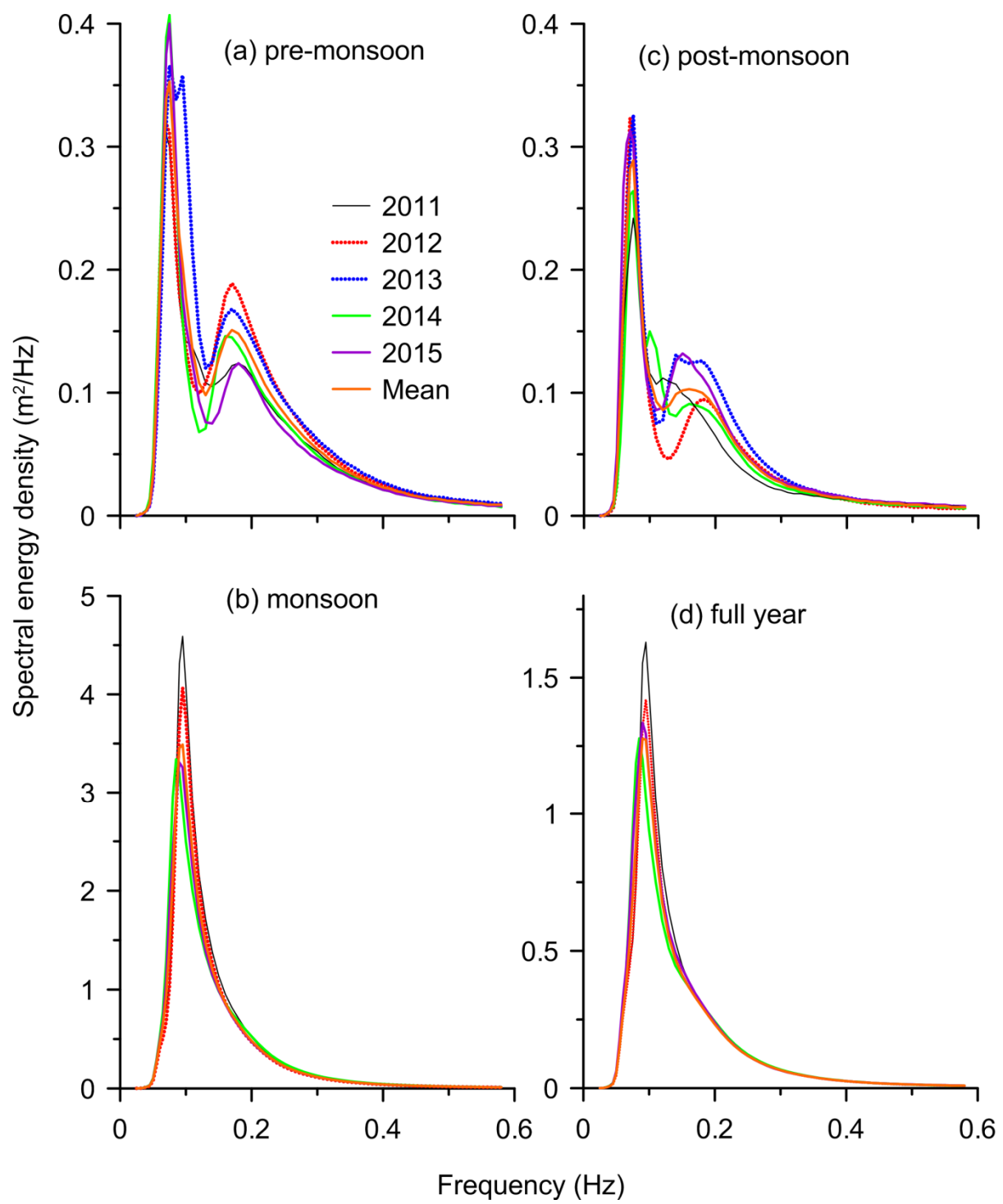


Figure 6. Monthly average wave spectra in 2011 to 2015



648



649

650

651

652

Figure 7. Wave spectra averaged over a) pre-monsoon (February-May), b) monsoon (June-September), c) post-monsoon (October-January) and d) full year in different years

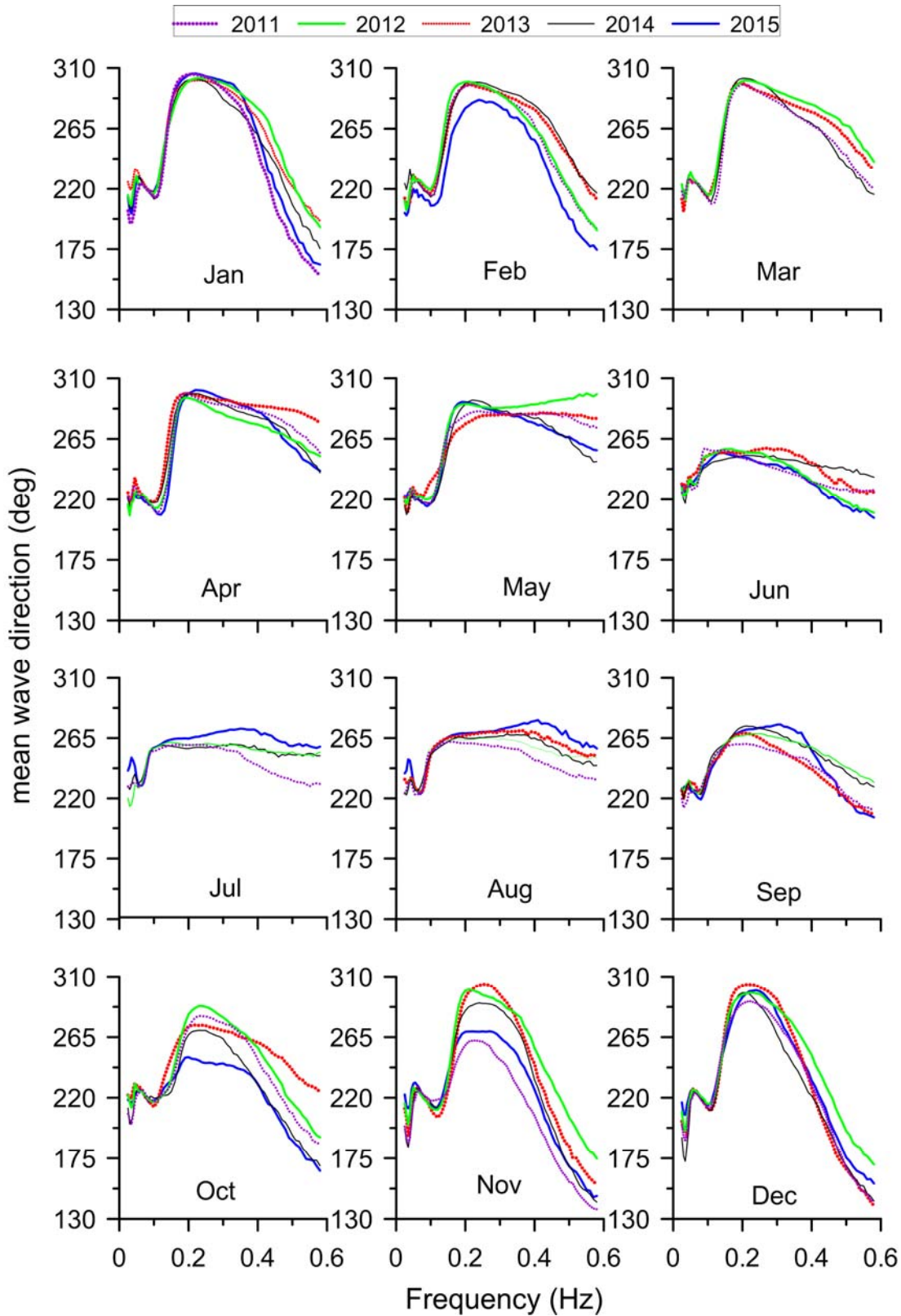


Figure 8. Monthly average wave direction at different frequencies in different months

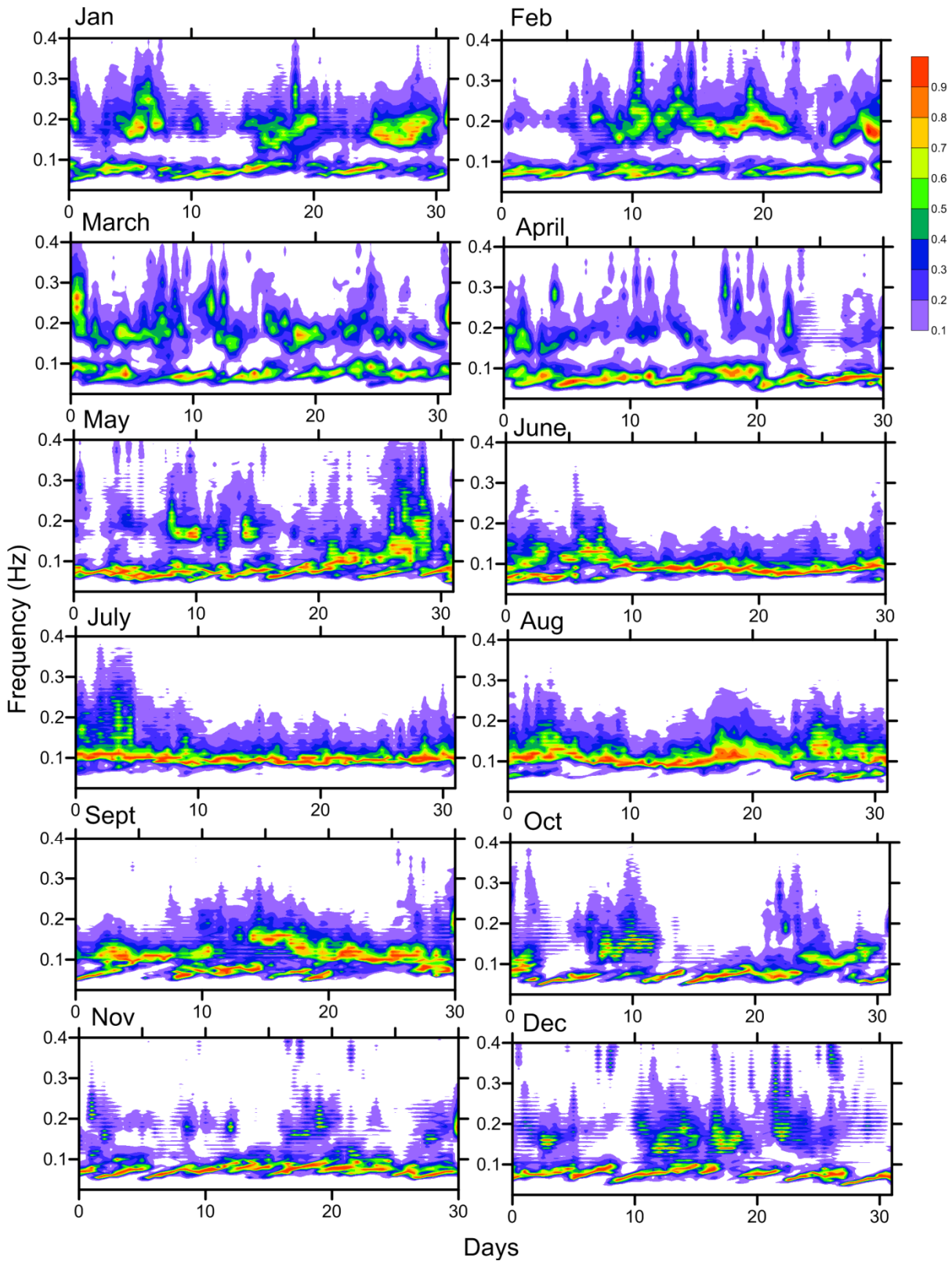


Figure 9. Temporal variation of normalized spectral energy density in different months (data from 2011 to 2015 used). The value used for normalizing the spectral energy density is presented in Fig. 2e.

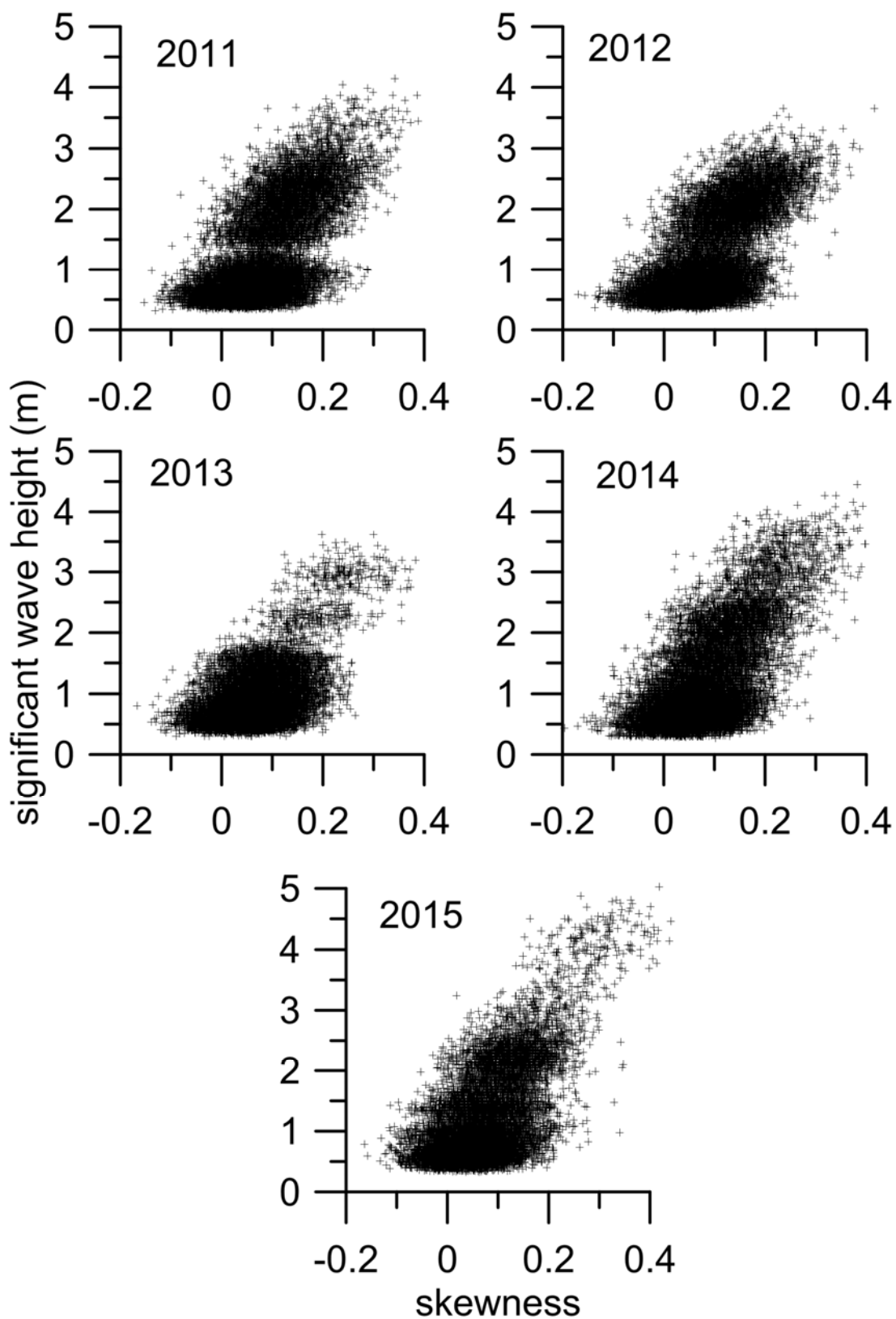
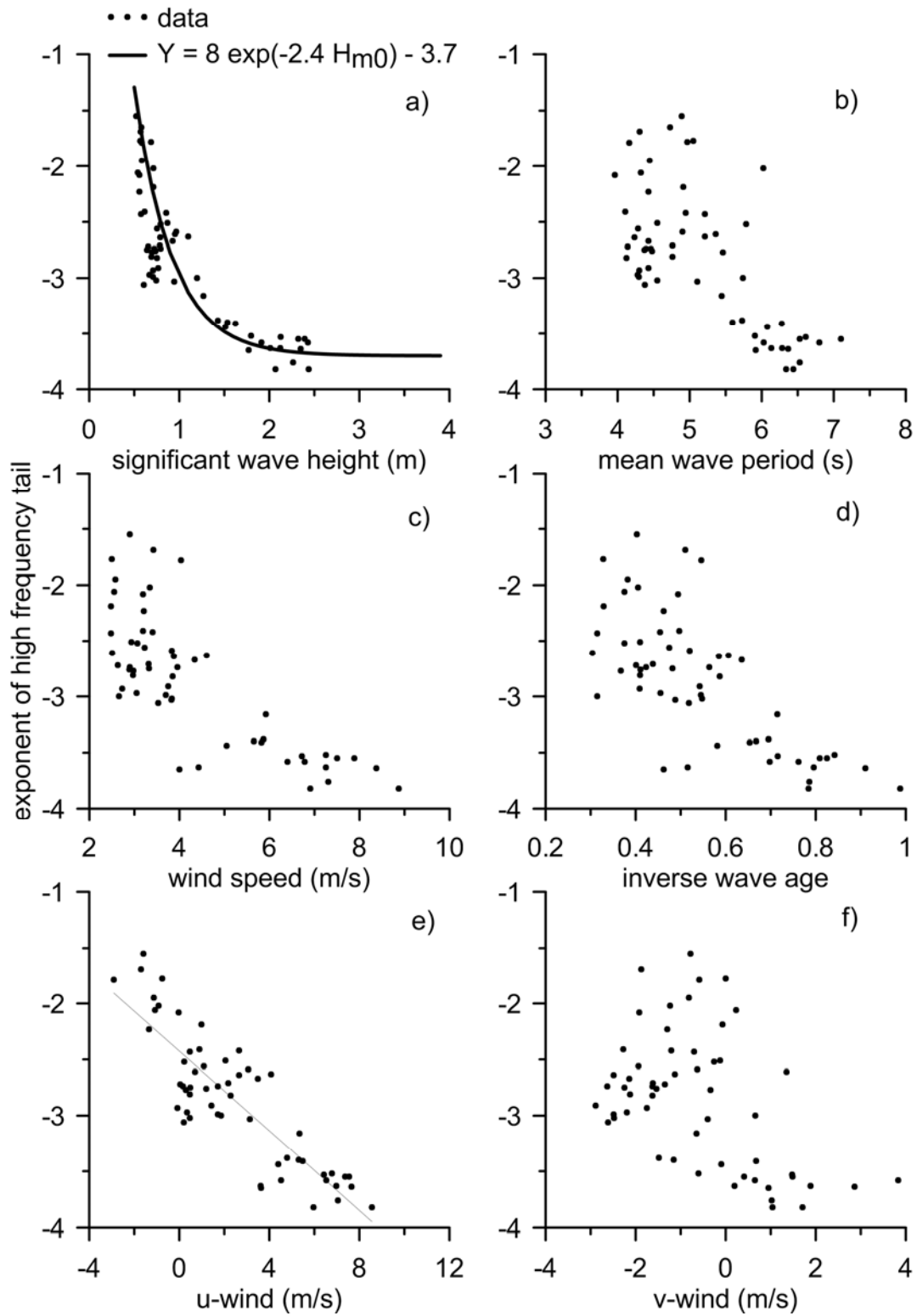
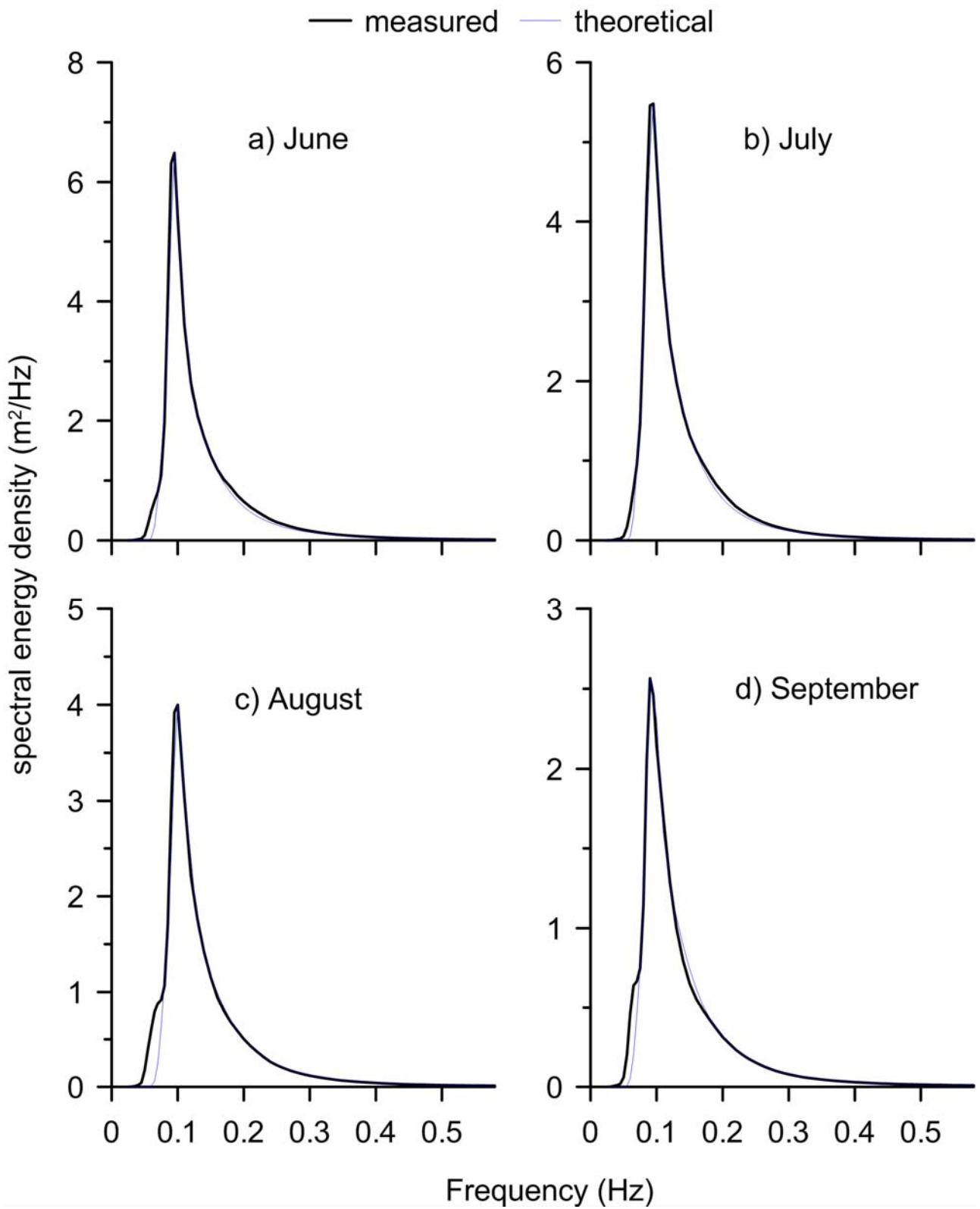


Figure 10. Scatter plot of significant wave height with skewness of the sea surface elevation in different years



666  
 667 Figure 11. Plot of exponent of the high-frequency tail with a) significant wave height b) mean wave  
 668 period, c) wind speed, d) inverse wave age, e) u-wind and f) v-wind



669  
 670 Figure 12. Fitted theoretical spectra along with the monthly average wave spectra for a) June, b)  
 671 July, c) August and d) September